Novel Quantification of Neurovascular Coupling (NVC) to Predict Brain Injury in Neonates with Hypoxic Ischemic Encephalopathy

by

Yudhajit Das

Presented to the Faculty of the Graduate School of

The University of Texas at Arlington in Partial Fulfillment

of the Requirements for the Degree of

DOCTOR OF PHILOSOPHY

THE UNIVERSITY OF TEXAS AT ARLINGTON

August 2020

Acknowledgements

First and foremost, I want to thank my advisor Prof. Hanli Liu for her constant support and patience in training me as a researcher. She taught me to think independently and solve problems innovatively. Her immense knowledge, professional guidance and powerful encouragement made my dissertation possible.

Furthermore, I would especially like to thank Dr. Lina Chalak for leading me into the field of Neonatal Encephalopathy. Her unique ability to combine medical problems and engineering solutions along with professional experience and knowledge guided me to find the optimized path to reach the goal in research. Also, I appreciate both Dr Lina Chalak and Dr Hanli Liu for their collaborative financial support in my Ph.D. experience.

My sincere thanks go to the rest of my committee members Drs. Rong Zhang, Srinivas Kota and Xinlong Wang for believing in me and guiding me with their insightful comments and encouragement throughout my Ph.D. journey, which incented me to widen my research from various perspectives. I appreciate all my committee members for their willingness to be my doctoral committee.

On top of that, I would like to express my appreciation to my colleagues Drs. Xinlong Wang, Srinivas Kota, Yulun Liu, and Fenghua Tian who provided me with a lot of useful innovative ideas and suggestions in data analysis and manuscript writing. Drs. Kota and Wang always extended their hands in my need, from introducing me to new scientific journals, debugging a code to interpretation of data. Dr. Yulun Liu helped me with statistical data analysis. Dr. Tian provided me with the initial help in understanding the clinical problems and taught me standardized approach to medical data analysis.

Apart from those aforementioned, I thank my senior/current lab colleagues Drs. Parisa Rabbani, Nghi Truong, Babawale Olajide, and Mrs. Akhil Chaudhari, Tyrell Pruitt, and Ms. Hashini Wanniarachchi for sharing their experience with me without any reservation.

Last but not the least, I would like to thank my mom, dad, sister, my uncle and his family and my girlfriend for their constant emotional support that has kept me going to solve challenging problems during every day and night!

August 12, 2020.

Abstract

Novel Quantification of Neurovascular Coupling (NVC) to Predict Brain Injury in Neonates with Hypoxic Ischemic Encephalopathy

Yudhajit Das, Ph.D.

The University of Texas at Arlington, 2020

Supervising Professor: Dr. Hanli Liu

Birth asphyxia is a global burden in clinical neonatal care. It results from deprivation of oxygen to a newborn infant that lasts too long during the birth causing physical harm to the brain. Hypoxic-ischemic encephalopathy (HIE) accounts for a significant proportion of encephalopathic newborns. The asphyxia insult impairs fetal cerebral blood flow and results in a distinctive neonatal encephalopathy (NE). Simultaneous measurement of near infrared spectroscopy (NIRS) and amplitude-integrated electroencephalography (aEEG) have been common tools for continuous monitoring of hemodynamics, cerebral perfusion and cerebral function of these asphyxiated neonates with fetal acidosis at the bedside. While the visual pattern of aEEG provides a gold standard tool for clinical practice, there is no methodology available to predict outcome of neurological or anatomical injury in neonates with HIE. My dissertation targets on this gap by developing novel quantification methods of neurovascular coupling (NVC) that are used to analyze concurrent recordings of NIRS and EEG from clinical cohorts of newborns with HIE.

First of all, the fact that no standardized algorithm exists for quantifying aEEG signal from raw EEG represents a significant challenge for the rigor of aEEG-dependent clinical analysis. To address this gap, Chapter 2 of my dissertation aims to examine whether variabilities in the aEEG outputs derived from various methods impact the determination of NVC, namely between aEEG and NIRS, in newborns with encephalopathy. A convenience sample with neonatal asphyxia were monitored for twenty hours in the first day of life with EEG and NIRS-based cerebral tissue oxygen saturation (SctO2). NVC between aEEG and NIRS-SctO2 was assessed using wavelet transform coherence (WTC) analysis, specifically by the wavelet total pixel number of significant coherences within 95% confidence interval. The raw EEG was converted

to aEEG using three different methods: Method (M1) derives from the algorithm by Zhang and Ding. Method (M2) uses a Neonatal EEG Analysis Toolbox (WU-NEAT). Method (M3) extracts output directly from a commercial platform with an undisclosed algorithm. The results demonstrate excellent agreement with Bland Altman comparisons for WTC-based NVC irrespective of the algorithms used. The findings of this study confirm the robustness of NVC wavelet analysis in NE related to HIE. Chapter 3 is a continuation work from Chapter 2 and specifically aims to further examine the rigor and consistency of novel neurovascular wavelet bundle methodology by evaluating the possibility of directly using raw EEG data for NVC assessment. Specifically, raw EEG and NIRS-SctO2 from the same sample of neonates as those reported in Chapter 2 are considered in Chapter 3. My results demonstrated excellent agreement of NVC assessment between the wavelet-metrics derived from SctO2-rawEEG coherence and those by SctO2-aEEG coherence using the three described aEEG algorithms, confirming that simple band-passed EEG can be paired with NIRS-SctO2 to assess NVC accurately in newborns with NE.

The severity of NE in HIE neonates is usually classified within 6 hours of birth into three stages as mild, moderate, and severe NE. These severity levels are correlated with the risk of disability and impaired cognitive development. It is critical to identify the newborns at specific severity levels so that appropriate therapies can be given promptly. There is a critical need to have real-time biomarkers for early prediction of brain abnormalities and severity in HIE infants for rapid treatment decision-making. To address this gap, Chapter 4 of my dissertation applies the novel neurovascular wavelet bundle methodology as a physiological biomarker to predict the presence of brain injuries in newborns as early as the very first day of life. Brain magnetic resonance imaging (MRI), considered as a proxy of neurodevelopmental outcome, was performed on all neonates (n=36) at a median age of 5 days; the entire cohort was grouped into two categories, with and without the evidence of neurological abnormalities and injuries. WTC analysis was performed to quantify NVC for a duration of twenty hours in the first day of life; wavelet metrics of percentage significant SctO2-aEEG coherence was compared between the normal and abnormal groups. The findings are significant and indicate that NVC-derived metrics measured in the first of life can be used as a physiological biomarker to accurately predict brain injuries seen a few days later by MRI, irrespective

of their original label as mild or moderate. Chapter 5 is an extension work of Chapter 4 and aims to investigate if NVC can also be used as a real-time physiological biomarker to discern among mild, moderate, and severe HIE neonates in the first day of life. Similarly, to Chapter 4, WTC-based NVC was performed on all the neonates between their SctO2 and aEEG signals, recorded in the first day of life and statistical analysis was performed. Although the assessment of the scale-dependent percentage of wavelet-based significant in-phase coherence showed different trends specific to each severity group, however, NVC-based metrics would not qualify as novel physiological biomarkers yet to stratify the severity of NE. Further investigation with a bigger sample size of each NE severity group is recommended.

Dynamic activities of the human brain share both linear and non-linear relationship between neuronal electrophysiology and brain hemodynamics, namely NVC. While NVC can determine the phase and amplitude coupling between aEEG and NIRS, they cannot detect the non-linear mechanisms affecting NVC. To the best of my knowledge, no study has utilized non-linear signal processing techniques to compute/quantify NVC in neonates. To address this gap, Chapter 6 discusses the future work of my dissertation where I explored dynamic time warping (DTW) as a non-linear method to monitor/quantify the NVC in neonates with HIE. Based on some preliminary results, I computed the predictive ability and shortcomings of DTW for identifying neonates with brain abnormalities in the first day of life. The findings suggest that DTW-derived relationships between aEEG and SctO2 may be a promising non-linear model fpr understanding the dynamic mechanism between electrophysiology and brain hemodynamics, guide therapeutic decision-making, or predict neurological outcome in HIE neonates in the first day of life, while further investigation and modal validation are needed.

Table of Contents

List of Illustrations

Chapter 1

Introduction

1.1.Background of Birth Asphyxia

Birth asphyxia is a global burden in clinical neonatal care. It results from deprivation of oxygen to a newborn infant (i.e. inability to establish inadequate/spontaneous respiration) that lasts too long during the birth process causing physical harm, usually to the brain. Every year four million newborns are affected worldwide, of which one million die and another million are left with disabilities. Hypoxic-ischemic encephalopathy (HIE) accounts for a significant proportion of encephalopathic newborns. The asphyxia insult impairs fetal cerebral blood flow and is manifested postnatally by a distinctive neonatal encephalopathy (NE), which is usually classified after birth using the clinical modified Sarnat stages as mild (with a score of 1-10), moderate (with a score of 11-14), and severe NE (with a score of 15-22). These sarnat scores correlate the risk for disability and impaired cognitive development with the severity of HIE.

1.2.Treatment and challenges

Hypothermia is a neuroprotective therapy to improve clinical outcomes by reducing body temperature of newborns for a specific duration of time. It is a standard of care for infants ≥36 weeks gestational age (GA) with moderate-to-severe HIE. The mild neonates (who usually have a normal outcome) do not meet the criteria for cooling and do not undergo hypothermia.

1.3.Conventional monitoring tools

Brain function and cerebral oxygenation in neonatal HIE have been monitored using multichannel standard EEG with two simplified analysis methods (i.e., amplitude integrated-aEEG and two-channel C3-C4 EEG) and near infrared spectroscopy (NIRS). These monitoring tools are highly desirable for clinicians to be able to assess severity of HIE on the bedside to quickly provide appropriate and timely interventions to prevent permanent injury of the neonatal brain.

1.4. Rationale of This Thesis

While the visual pattern recognition of aEEG provides a validated gold standard tool for the clinical use in sick newborns, there are no studies to date testing the effect of using different algorithms on the pattern recognition and its effect on clinical practice. For research purposes, similarly, there is no specific standardized algorithm method to quantify the aEEG signal from raw EEG data. The lack of transparency and multitude of algorithms generating aEEG signals can represent a significant challenge for the rigor of the clinical analysis that relies on aEEG processing, affecting both the clinical pattern recognition as well as research computations of neurovascular coupling based on upper and lower margins of aEEG voltage. Another big and concerning gap in neonatal encephalopathy remains in the early prediction of brain abnormalities. Even following the introduction of hypothermic therapy, approximately 40% of newborns still have neurodevelopmental abnormalities at 24 months of age. Recent reports also suggest new evidence of cognitive impairment in a subset of 30–50% of "mild NE" cases, who are currently not recognized during postnatal classification and therefore not offered any therapies. While adjuvant therapies are being sought, an important focus of research is to recognize which neonates need therapies to improve outcome, the ability to quantify coupling of NIRS and EEG in HIE in real time has received very little attention. To address all these gaps, overall, this dissertation will focus on few aims.

My first aim is to investigate the effects of different aEEG algorithms on WTC, and the second aim is to overcome the prior limitations and use dynamic wavelet coherence to determine potential biomarkers to predict early brain abnormalities. Such biomarkers may be used to clinically discern between mild and moderate NE severity within a short therapeutic window after birth and to better understand the pathophysiological mechanisms of HIE-related brain injury. Also, such biomarkers can be essential for developing new effective interventions to improve clinical outcomes. However, a few limitations of WTC analysis exist, including (1) long time recording of NIRS and EEG signals to accurately quantify wavelet metrics of a wide range of very low frequency oscillations, (2) long processing time of WTC analysis following full recording of signals, and (3) non-feasibility of

implementation at bedside because of required long data-processing period. To overcome these drawbacks, my third aim of this study is to investigate the feasibility of using non-linear time alignment as an alternate method that can potentially facilitate real-time bedside monitoring of neurovascular coupling in neonates with HIE.

1.5. Organization of This Thesis

This dissertation has 6 chapters, which consist of one peer reviewed publication (Chapter 1), and three manuscripts that are ready to submit (Chapter 3, 4 and 6). Chapter 1 is a brief introduction of the birth asphyxia, current treatment and challenges, conventional monitoring tools and need for biomarkers to guide therapeutic decision-making and early prediction of brain abnormalities. Chapter 2 investigates if the multitude of differences in available EEG signal processing algorithms matter in the assessment of Neurovascular Coupling (NVC) in Newborns. Chapter 3 aims to study if raw EEG can be used instead of aEEG in NVC assessment. In Chapter 4, assessment of the scale-dependent percentage of wavelet-based significant coherence is done to stratify the spectrum of encephalopathy severity in HIE neonates with normal and abnormal MRI outcomes in first day of life. Chapter 5 investigates the feasibility of using NVC as a biomarker to clinically discern between mild, moderate, severe NE severity within a short therapeutic window after birth. Finally, chapter 6 investigates if a non-linear measure using dynamic time warping can be used to stratify severity of encephalopathy in the first day of life.

Chapter 2

Rigor of Neurovascular Coupling (NVC) Assessment in Newborns Using Different Amplitude EEG Algorithms

This chapter is a publication at the journal of Scientific Reports, vol. 10, p. 1-9, 2020)

Authorship: *Yudhajit Das[1], Hanli Liu[1], Fenghua Tian[1]; Srinivas Kota[2], Rong Zhang[3], and Lina F Chalak[4*]*

2.1. Introduction

The amplitude-integrated EEG (aEEG) has become a very useful clinical device in newborns; new systems are continuously enriching the market with variable algorithms not always disclosed by free access to the public. While the visual pattern recognition of aEEG provides a validated gold standard tool for the clinical use in sick newborns [1,2], there are no studies to date testing the effect of using different algorithms on the pattern recognition and its effect on clinical practice. For research purposes, similarly, there is no specific standardized algorithm method to quantify the aEEG signal from raw EEG data.

The lack of transparency and multitude of algorithms generating aEEG signals can represent a significant challenge for the rigor of the clinical analysis that relies on aEEG processing, affecting both the clinical pattern recognition [3,4] as well as research computations of neurovascular coupling based on upper and lower margins of aEEG voltage [4,5]. We have recently reported a novel quantification of neurovascular coupling (NVC) using a wavelet transform coherence (WTC) analysis on the dynamic signals of aEEG and cerebral tissue oxygen saturation (SctO2) in neonatal encephalopathy [4] where time series from a selected pair of electrodes was directly processed as output from a commercial device.

The current proof of concept investigation aims to further examine the rigor and consistency of the novel WTC analysis for NVC quantification by evaluating the effects of using three different aEEG algorithms to process the raw EEG recordings obtained from infants with neonatal encephalopathy. We compare the variability observed with the three algorithms with respect to (1) aEEG tracings with upper

and lower margin amplitudes which affect the clinical background pattern, and (2) research-based, WTC-derived metrics of neurovascular coupling NVC.

2.2. Materials and methods

2.2.1. Study population and measurement protocol

To test the effect of the different data-processing algorithms, we selected a convenience sample of eight newborns with hypoxic ischemic encephalopathy (HIE) who had twenty hours of EEG monitoring as a standard of care protocol. Infants had a birthweight of ≥1800 g, were ≥36 weeks of gestation, and admitted to the neonatal intensive care unit at Parkland Hospital, Dallas, TX with evidence of fetal acidosis and encephalopathy. Infants had normal MRI outcome and none of these infants had seizures during their recording period. The aEEG and regional cerebral tissue oxygen saturation (SctO2) by near infrared spectroscopy (NIRS-SctO2) of all neonates were simultaneously recorded during the entire course of 20-hour monitoring, which made it feasible to perform dynamic wavelet coherence analysis. Eight EEG electrodes were placed on the newborns' scalps at C3, C4, P3, P4, O1, O2, Cz, and Fz, according to the 10-20 international system. EEG signals from all 8 electrodes were recorded at a sampling rate of 256 Hz and then amplified and filtered within a frequency band of 0.1-100 Hz. Both EEG and NIRS-SctO2 signals were interfaced with a multi-device synchronization platform (**Moberg Research, Inc., PA, USA**) for simultaneous recording of two modalities and then saved for off-line analysis using MATLAB (Mathworks, Inc., MA, USA). The study was approved by the Institutional Review Board of the University of Texas Southwestern Medical Center and informed consent was obtained from parents of each newborn before enrollment.

2.2.2. Data preprocessing for three methods to acquire aEEG

As mentioned earlier, recent commercial EEG systems from different medical device manufacturers have often embedded aEEG modules. While they continuously provide clinicians with advanced and convenient tools, each has their own undisclosed algorithms to obtain aEEG for targeting on specific medical applications of neonates. In general, these methods or algorithms share common steps to

preprocess raw EEG data before making the conversion to aEEG which are transparent and briefly summarized below, with a schematic comparison shown in Fig. 2-1. A finite impulse response (FIR) band-pass filter was used to eliminate low-frequency physiological artifact and to attenuate high-frequency signals over 20 Hz that can arise from muscle activity, power line interference, and other unwanted noises. This filter was digitally implemented to mimic the analog filters of Cerebral Function Monitor (CFM), slightly attenuating the dominant delta-wave patterns [3]. The filtered signal was next passed through a peak sensitive rectifier for peak-to-peak rectification, followed by a peak detection and data smoothing algorithm.

After these common steps, different data processing algorithms for quantifying aEEG are used depending on the device and manufacturer, which are not standardized and often not even disclosed [3,6]. To examine the effect of different aEEG tracing algorithms on the NVC analysis in this study, we used two published algorithms and compared them with an additional third commercial platform/device (Moberg) algorithm. Specifically, the three methods used are summarized below:

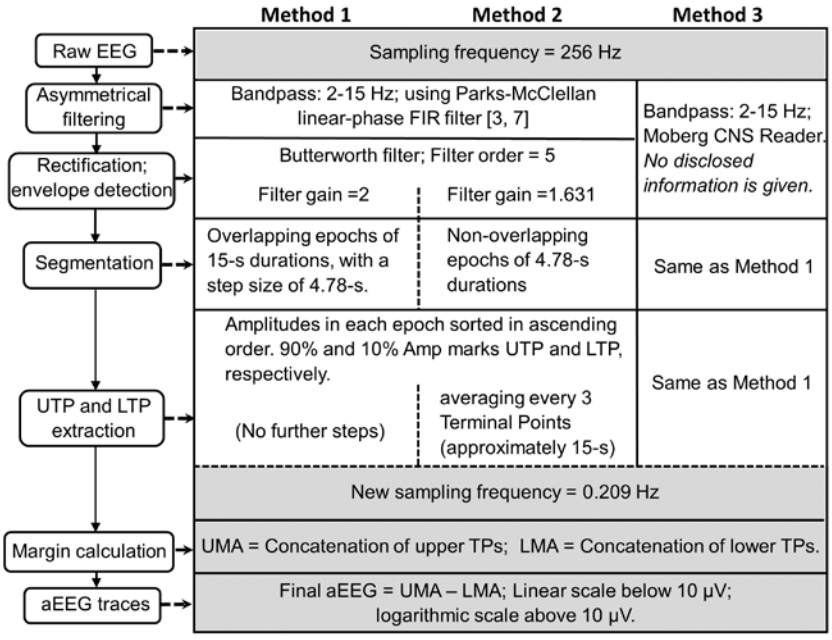

Figure 2-1. Overview of different steps among three algorithms, showing how to obtain the same sampling rate for aEEG and NIRS. TPs: terminal positions; UTP: upper terminal positions; LTP: lower terminal positions; UMA: upper margin amplitudes; LMA: lower margin amplitudes.

2.2.2.1. Method 1 (M1)

This method was based on the algorithm reported by Zhang and Ding, with a step-by-step signal-processing approach to calculate aEEG upper and lower margins from raw EEG data [3].

Step 1 - Asymmetrical filtering: An asymmetrical, flat band-pass, linear phase FIR filter was designed using Parks-McClellan algorithm [7] to compensate the attenuated energy of nonrhythmic components at each frequency [3]. This filter enabled us to perform weighted amplification to EEG signals in the frequency range of 2 - 15 Hz, while simultaneously attenuating low-frequency artifacts.

Step 2 - Rectification: The asymmetrically filtered data were then passed through a peak-sensitive rectifier to undergo full wave rectification for evaluation of the absolute value/amplitude.

Step 3 - Envelope detection: Since the boundary or envelope of the EEG waveform is the key to characterize the tendency of amplitude changes, envelope detection was implemented using a 5^{th} order Butterworth filter. This process enabled to extract a smooth curve approximately drawn through the peaks of the rectified EEG tracings and concisely outlined the amplitude feature of the raw EEG signals. A gain factor of 2 was then applied on the envelope when obtaining 256 Hz aEEG signal.

Step 4 - Time-amplitude compression: This last step was designed to achieve a bird's-eye overview of the long-term aEEG tracing. This part of processing in our method was slightly modified from the original paper to achieve a target sampling frequency of 0.209 Hz, the frequency used in acquiring SctO2 signal from the newborns, in order to perform NVC between them. Thus, instead of taking a non-overlapping sliding window of 15 s [3], we segmented the envelope of the rectified EEG into overlapping epochs of 15-s durations in order to compress the envelope tracing in time (time-scale reference: 6 cm/h). The amplitudes in each epoch were thereafter sorted in ascending order of amplitude. The maximum and minimum amplitudes in each epoch should ideally be chosen as upper and lower terminal points

respectively. However, in order to ensure robustness of the algorithm against high and low amplitude noises, the 90th and 10th percentile of the sorted data was defined as the UMA and LMA values for each 15-s sliding, rectangular time window. Choosing an overlap time of 10.22 s for the sliding window, we obtained maximum and minimum peak extractions in each 4.78-s duration, termed as upper and the lower terminal points of the associated aEEG tracings. A vertical line was made for each pair of each upper and lower terminal points to represent a 4.78-s epoch. Then, a curve was drawn through the peaks and troughs, respectively, to obtain smooth upper and lower representative aEEG upper and lower margins. In this way, we were able to achieve a sampling rate of 0.209 Hz (i.e., 1 data point per 4.78 s), which matched the acquisition rate of SctO2 signal, for performing WTC. The processed aEEG tracings were plotted using a semi log-scale (i.e., base 10) for y-values larger than 10 µV to reduce the dynamical range of large fluctuations of raw EEG, while keeping a linear scale for y values between 0-10 µV to accurately depict the low amplitudes. By the end, the time-varying tracings of differences between UAM and LAM were used for aEEG values to quantify WTC and thus NVC.

2.2.2.2. Method 2 (M2)

This method made use of Washington University-Neonatal EEG Analysis Toolbox (WU-NEAT)[6]. WU-NEAT is an open source, MATLAB-compatible, clinically validated toolbox; it is encapsulated in an easy-to-use GUI to quantify both aEEG and spectral edge frequency for assisting collaborative research in neonatal EEG with limited channels [6]. We utilized WU-NEAT as a second method/algorithm, M2, to calculate aEEG from our raw EEG data. The processing steps were similar to those in M1 and are briefly summarized as three steps, as follows:

Step 1 - Asymmetric filtering***:*** raw EEG data were first passed through an asymmetric band-pass filter (Parks-McClellan linear-phase FIR filter), strongly attenuating the signal below 2 Hz for low-frequency physiological artifact, such as respiratory and heart artifact, and above 15 Hz to remove muscle activity and power line noise. The band-passed signals within 2-15 Hz underwent gradual amplification

with a slope of 12 dB/decade to compensate for the diminished amplitude due to the scalp and skull attenuations.

Step 2 - Rectification and envelope detection***:*** Similar to M1, the band-passed EEG signals were rectified, followed by envelope extraction using a 5^{th} order low-pass Butterworth filter with zero-phase filtering. The resulting aEEG tracings were obtained by applying a gain of 1.631 on the envelope.

Step 3 - Time-amplitude compression: The resulting processed signals (with a 256-Hz sampling rate) after Step 2 were down-sampled to 0.209 Hz to match that of SctO2 signal measured in our study. The original method in WU-NEAT recorded upper and lower terminal points in every 3.12 s, followed by a simple moving average over 5 such adjacent terminal points to form a smoothed 15-s epoch. We modified this down sampling technique by segmenting each 256-Hz, 15-s EEG epoch into five of 3-s epochs, followed by calculation of the maximum and minimum amplitudes in each epoch, which contained 768 adjacent EEG data points (=3 s × 256 Hz = 768). The amplitudes of the 90^{th} and 10^{th} percentile of the sorted data was defined as the upper and lower terminal points to represent each 3-s epoch. Next, in order to time-compress the 256-Hz aEEG signals, a simple overlapping moving average with a step of 4.78-s was performed over every 5 upper and lower adjacent terminal points (or covering 15-s epoch) to obtain smoothed aEEG tracings. As M1, a linear scale was used from 0-10 μV and a semi-log scale used from 10-100 μV, following the conventional aEEG presentation format.

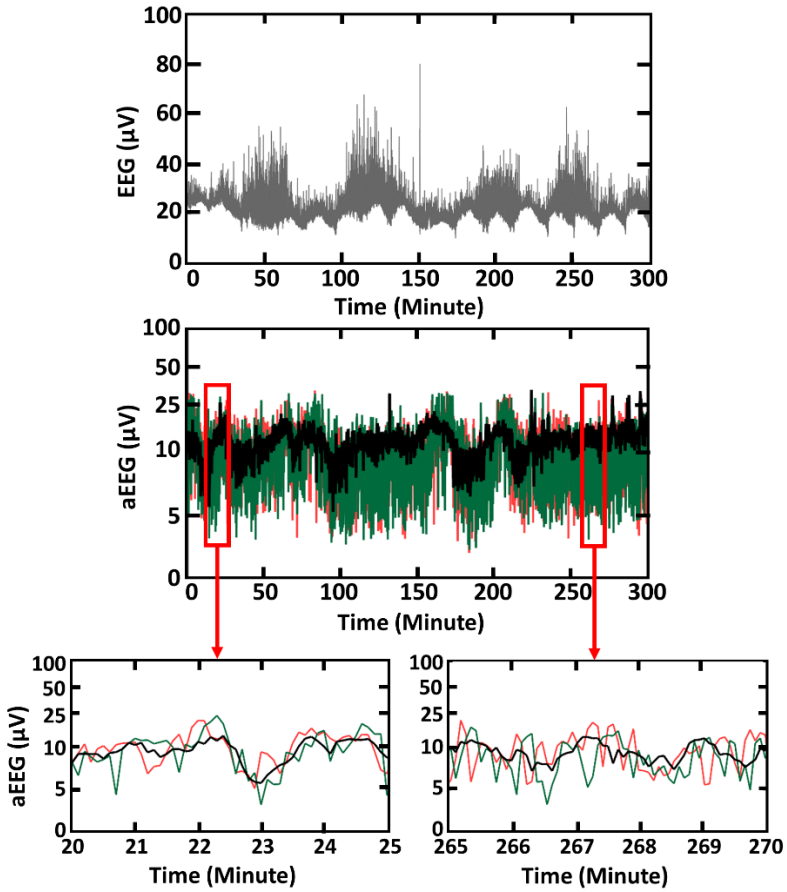

Figure 2-2. Top illustrates an example of 5-hour raw EEG tracings recorded with a 256-Hz sampling frequency. Middle shows 3 aEEG tracings obtained using M1 (red), M2 (black), and M3 (green). Last shows two highlighted sections of 5-minute each, segmented from the same aEEG tracing derived from M1(red), M2 (black), and M3 (green), respectively.

2.2.2.3. Method 3 (M3)

Direct aEEG output tracings were attained from a commercial synchronization platform with undisclosed algorithm (CNS Reader, Moberg ICU Solutions, Ambler, PA). Moberg ICU Solutions is a medical device manufacturing company that specializes in neuromonitoring and patient information management. The Component Neuromonitoring System (CNS Monitor) is commercially available to display multiple clinical/vital parameters that are collected simultaneously from various medical devices. CNS Reader is a

Windows-based software application designed as a companion to the CNS Monitor that facilitates data collection, data recording, and data analysis for multimodal devices, with a focus on EEG.

Step 1 and 2 – Pre-processing and Conversion of 256-Hz EEG data into aEEG with the same frequency**:** CNS Reader has inbuilt functions that automatically perform band-pass filtering (2–15 Hz) followed by line noise removal, rectification, and detection of the amplitude margins on raw EEG data. The output parameters of CNS-processed aEEG can be downloaded as a data file for further off-line analysis in MATLAB. The process or algorithm of conversion from raw EEG into aEEG (Step 1 and 2) has not been disclosed by the company. The 256-Hz aEEG tracings directly outputted from the CNS Monitor/Reader were downloaded for our next-step analysis.

As shown in Fig. 2-1, all the processing steps (i.e., ***Step 3*** to ***Step 6***) in M3 were the same as M1.

As an example, Fig. 2-2 top shows a trace of 5-hour raw EEG signal, sampled at 256-Hz from a normal reference control neonate. The y-axis of this figure represents amplitude of pre-processed EEG in micro-volt and is plotted with a linear scale, while x-axis represents time in minute. Fig. 2-2 middle shows three aEEG tracings derived from the EEG trace shown above using M1 (red), M2 (black), and M3 (green), respectively. To clearly examine the differences among three aEEG curves, we extracted two-time segments with a period of 5-minutes for each. This example is consistent with previous reports[5] and illustrates how even though all three aEEG were derived from the same EEG tracing, the amplitudes and/or envelop values of the aEEG vary amongst the three methods.

2.2.3. Quantification of NVC using the wavelet transform coherence (WTC) statistical methods

To determine whether variations in aEEG tracings affect the NVC between aEEG and SctO2, we used WTC analysis of spontaneous oscillations of aEEG and NIRS-SctO2 as we recently published in Neonatal Encephalopathy (NE)[4]. A 95% confidence interval was chosen to identify regions of interest (ROIs) within the time-scale map. These ROIs mark or label statistically significant coherence reflecting NVC across different times within an upper to lower scale range for each of the three SctO2→aEEGs pairs. Specifically, we used a MATLAB-based software package[8] to perform WTC analysis between the

spontaneous oscillations of NIRS SctO2 and aEEG (SctO2→aEEG) derived each from the same raw EEG time series using each of M1, M2 and M3, respectively, marked as SctO2→ $aEEG_{M1}$, SctO2→$aEEG_{M2}$, and SctO2→$aEEG_{M3}$. Using a time-scale (equivalent to time-frequency) domain, NVC was assessed by wavelet metric estimation of total pixel number of significant coherence.

Further, to quantify NVC results derived from three different aEEG methods, we introduced, implemented, and assessed a WTC-derived index in the time-scale domain, *Pix*. Specifically, we denoted the pixel number of significant coherences across all total scales (Pix_{total}). All pixels that had values of squared cross-wavelet coherence R^2 significantly higher than the simulated background noise ($p < 0.05$) were identified and marked as statistically significant coherence contours[8]. Then, we quantified Pix_{total} by summing respective pixel numbers across all wavelet time scales within the entire WTC time-scale domain (outside of the cone of inference, COI)[8]. Finally, a coefficient of variation (*COV*) was introduced to evaluate levels of variation and/or effect of different aEEG algorithms on WTC-based NVC.

COV was defined as $COV = \frac{SD}{mean\ of\ significant\ coherence\ Pixels}$, where *SD* stands for standard deviation of significant coherence pixels across entire scale from the mean values of significant pixels averaged over those determined with the three algorithms.

Statistical analysis to compare methods agreement was performed using Bland Altman curves to detect differences larger than one standard deviation from the mean.

2.3. Results

2.3.1. Effect of the processing algorithm on the clinical pattern of the aEEG

We quantified three aEEG tracings in a convenience sample of eight newborns with HIE across 20 hours of monitoring period in the first day of life using the three aEEG algorithms. As an example, Fig. 2-2 shows a comparison of the time and time-scale domain quantifications from neonate #N1 of different aEEG traces along with SctO2 signal recorded simultaneously with the EEG signal. It highlights a large variability from using each of M1, M2 and M3 in both lower and upper amplitude margins of these tracings. Specifically, aEEG curves obtained in the same patient using M2 produced a narrow bandwidth

and a normal continuous pattern, while M1 or M3 resulted in a discontinuous tracing. The example highlights how the discrepancies in algorithm can result in a different aEEG pattern in the same patient, each being associated with a different therapy and prognosis implication.

2.3.2. Effect of the processing algorithm on research WTC-derived NVC

Next, we performed time-frequency analysis of the three aEEG tracings derived from M1, M2 and M3, as well as their respective SctO2 signal using continuous wavelet transform (CWT) and analytic Morlet wavelet[8]. The corresponding time-frequency spectrograms are shown in Fig. 2-2(e-h), where the x-axis represents time in hours, the y-axis represents frequency in mHz, and the color scale represents the amplitude of power after CWT. Despite the variability in aEEG tracings in Fig. 2-2(a-c), consistent patterns are demonstrated in the frequency range of 0.1 mHz to 2 mHz with the spectrograms obtained from the three algorithms marked by dashed lines in Fig. 2-2(e-g), as well as for the SctO2 spectrogram (Fig. 2-2(h)).

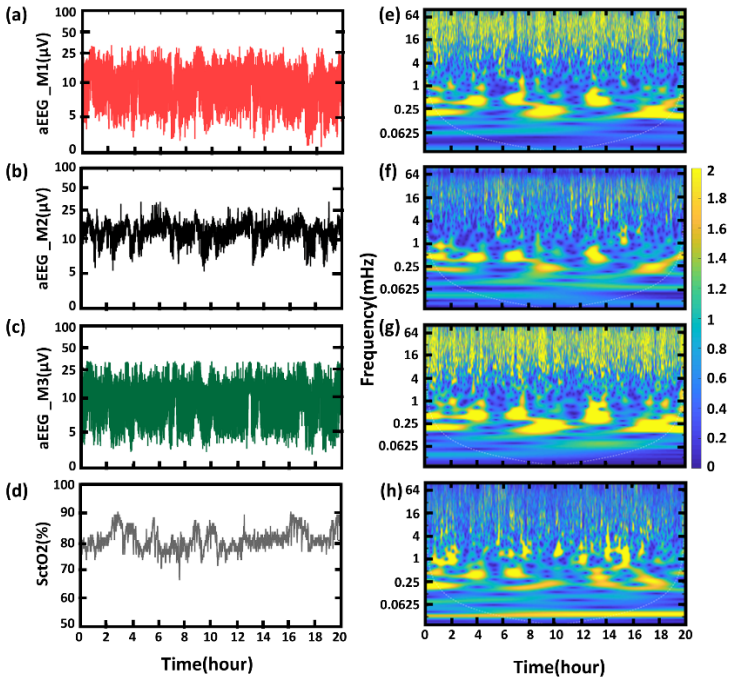

Figure 2-3. An example of three aEEG tracings in μV obtained using (**a**) M1, (**b**) M2, and (**c**) M3 of a

neonate (neonate #1) with normal MRI outcome. (**d**) SctO2 signal recorded simultaneously. (**e**–**h**) Wavelet transformation of the corresponding aEEG tracings derived using (**e**) M1, (**f**) M2, (**g**) M3 and (**h**) SctO2, respectively, where y-axis represents Frequency in mHz, and the color represents the amplitude of power after CWT.

Furthermore, the WTC-based time-scale coherence maps/spectrograms obtained from the same above patient highlighted various aEEG pattern interpretation (#N1) are illustrated in Fig. 2-3 red box, comparing effects of three aEEG processing methods on NVC. The figure highlights the consistent time-scale patterns between aEEG and SctO2 represented in the scale range of 640-10240 s (0.1 – 1.6 mHz).

At the group level, Fig. 2-3 shows the corresponding time-scale coherence of NVC, R^2, for all eight neonates highlighting a full range of NVC. Notably, neonates N1-N4 have high NVC coherence while neonates N5-N8 have lower NVC. Despite the large physiological NVC variability observed within multiple patients, consistent coherence patterns were observed specifically in the scale range of 640-10240 s for each neonate depicted, regardless of the aEEG processing methods used.

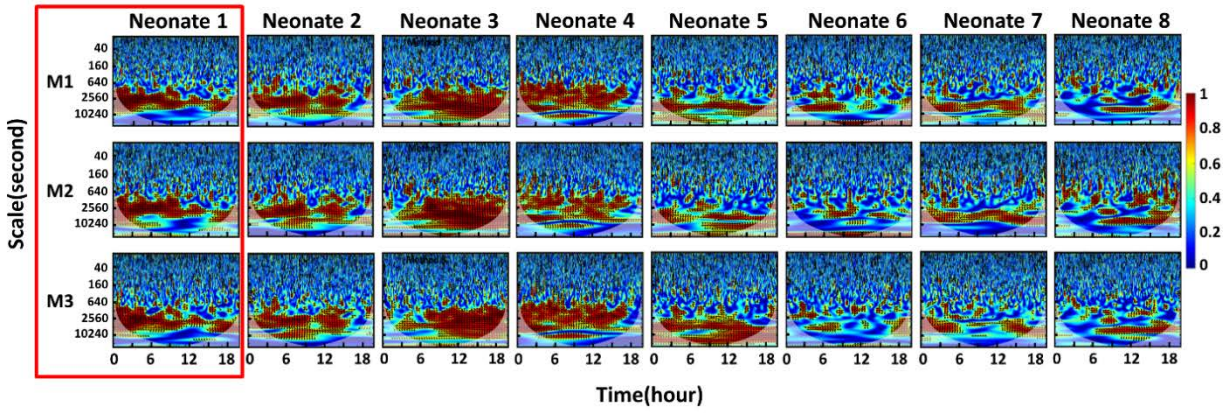

Figure 2-4. Time-scale coherence maps of NVC in the selected cohort. The x-axis represents time in hours, the y-axis represents scale in seconds, and the color scale represents the amplitude of WTC coherence, R^2. The areas with significant NVC ($p < 0.05$) are contoured with black lines and filled by red color within the time-scale WTC maps. WTC-based SctO2-aEEG coherence (R^2) are plotted for each one of the 8 neonates (Neonate #: N1- N8). Each vertical column represents the results derived from three

aEEG methods, respectively, highlighting the similarity in NVC pattern for each newborn among $R_{SctO2 \rightarrow aEEG\_M1}$, $R_{SctO2 \rightarrow aEEG\_M2}$, and $R_{SctO2 \rightarrow aEEG\_M3}$.

2.3.3. Calculation of the total number of pixels within statistically significant contours across entire scale

Figure 2-5(left) tabulates the total numbers of pixels that are significantly coherent between SctO2 and aEEG identified by 3 methods across entire scale (Pix_{total}) and the corresponding *COV* values ranging from 2.01% (Neonate 1) to 14.34% (Neonate 8) for the entire scale. This highlights that high significant coherence with more pixels (such as in N1-N4) is associated with a smaller *COV* value. Fig. 2-4(right) plots the total number of significant pixels, Pix_{total}, identified by method M1, M2 and M3, versus respective *COV* values for all 8 neonates, demonstrating a negative linear relationship. Fig. 2-5 indicates that variations in WTC-derived NVC caused by different aEEG algorithms are associated with the degree of NVC between aEEG and SctO2. Stronger NVC is associated with the least variation caused by aEEG algorithms.

	#pixels_M1 ($x10^5$)	#pixels_M2 ($x10^5$)	#pixels_M3 ($x10^5$)	Mean ($x10^5$)	SD ($x10^5$)	Coefficient of Variation (%)
Neonate 1	5.09	5.12	5.28	5.16	0.1	2.01
Neonate 2	5.67	5.16	5.19	5.34	0.28	5.29
Neonate 3	6.62	6.87	6.05	6.51	0.42	6.44
Neonate 4	6.56	5.93	6.82	6.44	0.46	7.13
Neonate 5	4.43	4.44	5.35	4.74	0.53	11.13
Neonate 6	4.18	3.47	3.22	3.62	0.5	13.76
Neonate 7	4.52	4.86	3.66	4.35	0.62	14.23
Neonate 8	3.71	4.5	3.42	3.88	0.56	14.34

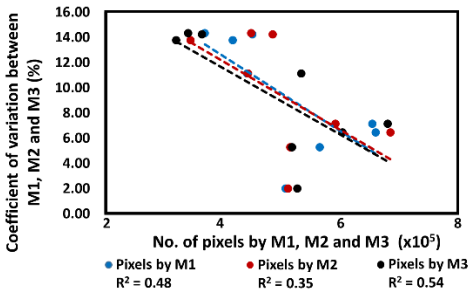

Figure 2-5. (Left)- Total number of significant coherence pixels derived with M1, M2 and M3 across the entire scale (*Pixtotal*) for each of eight neonates. (Right)- Relationships of total number of significant pixels (*Pixtotal*) derived by M1 (blue), M2 (red) and M3 (black) vs respective *COV*s. Dashed lines represent color-matched regression lines for each case.

We utilized Bland-Altman plots to compare the total number of significant coherence pixels (#_pixels) over the entire wavelet scale range by M1, M2 and M3, as shown in Fig. 2-6(a-c). Results indicate that the differences in #_pixels are within the one standard deviation limit for all neonates

regardless of the pair of methodology M1 vs. M2, M1 vs. M3, or M2 vs. M3. This observation implies that regardless of differences in aEEG processing algorithms, a significant level of agreement/consistency on WTC-based NVC (i.e., SctO2-aEEG coherence) exists based on the total number of significant coherence pixels across the entire wavelet scale. Furthermore, Fig. 2-6(d-f) panels demonstrate the consistency of numbers of significant coherence pixels determined by each pair of the three methods, by linearly regressing against a "line of identity". Overall panels in Fig. 2-6 indicate the robustness of the WTC-based NVC based on the total number of significant coherence pixels across the wavelet scale, irrespective of the aEEG algorithm differences during the duration of the monitoring period.

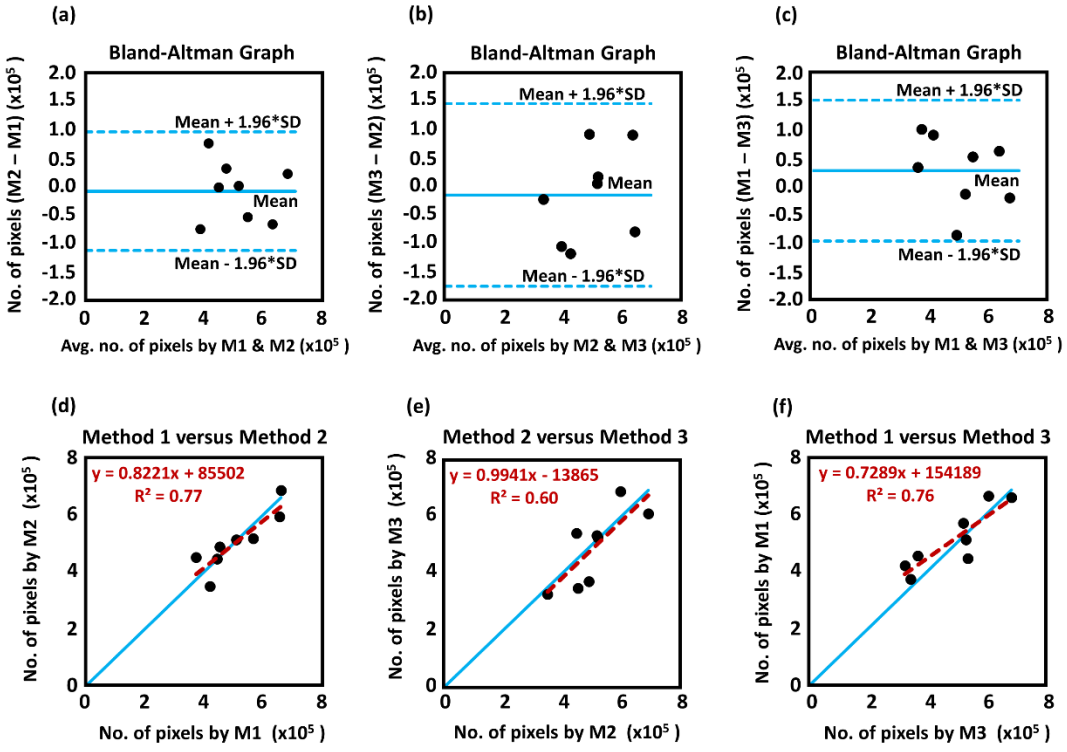

Figure 2-6. Comparison of WTC results based on aEEG values derived from M1, M2, and M3 using the entire range of wavelet scale. (**a**–**c**) Bland-Altman plots to compare WTC agreements between paired aEEG methods: (**a**) M1 vs. M2, (**b**) M2 vs. M3, and (**c**) M1 vs. M3. The horizontal upper and lower blue lines mark the limits of agreement, defined as the mean difference ± 1.96 SD. (**d**–**f**) A comparison of total numbers of significant coherence pixels derived from paired aEEG methods: (**a**) M1 vs. M2, (**b**) M2 vs.

M3, and (**c**) M1 vs. M3. A blue "line of identity" is given in each panel as perfect match between the results from the two respective methods. The red line in each panel shows the linear regression.

2.4. Discussion

We have established a new neurovascular wavelet bundle methodology which enables an unprecedented real time analysis of neurovascular coupling non-invasively at the bedside.[4] Key finding highlighted in this study is the robustness of NVC based on WTC analysis between aEEG signal and SctO2 in newborns with encephalopathy irrespective of differences in processing algorithms leading to variability in aEEGs. In order to measure the neurovascular coupling with rigor, it is important that the dynamics of the signals are matched carefully. In general, biomedical signals arise from a variety of sources such as electrical activity of neurons (EEG/ aEEG) and optical absorption of light (NIRS). Due to the different sources, biomedical time series are typically associated with different time scales of operation. An EEG signal, for example, changes rapidly due to the (de)synchronization of numerous neurons, while a NIRS signal only changes very slowly, due to the fact that the hemodynamic slow time scale.[9]

While all three EEG to aEEG conversion methods follow common pre-processing steps, such as asymmetrical band-pass filtering, rectification and envelope detection, each has a different frequency filter designs and peak detection settings for aEEG tracing generation from raw EEG signal. Such differences include the order of filters, the value of gain, induced ripples along with the passband filter, window durations and terminal selection for peak detection, as well as the degree of smoothing. In principle un-identical filters will generate un-identical waveforms. Furthermore, the use of a filter always has a tradeoff between the frequency response and time response. The amount of signal alteration caused by filters depends on the degree of dissimilarity between methods. The above explains why different algorithms have resulted in significant differences in shape and amplitude margins of the aEEG output. This is consistent with the literature[5] and could impact clinical care as highlighted in select example. The effect of the resulting differences in bandwidth shape and voltage on the full aEEG interpretation in both health and disease has not been studied to date. Importantly one must be aware of the filter settings at the

bedside and how this affects when serial comparisons when different filters are selected that impede further comparisons. Our results agree with findings by Werther et al [5], which highlight the importance of careful selection of filters and band-pass range that can affect the tracing interpretation.

These differences could be minimized by awareness of this particular issue and a careful selection of the algorithm settings[5]. The latter is not possible if these algorithms are undisclosed in commercial devices. These findings indicate that the aEEG pattern classification from automated tools cannot not recommended for clinical decision making at the present time and that vendors must be required to disclose details of their aEEG algorithm.

Despite the variabilities in the shape and amplitude margins of the aEEG output, we observed consistent patterns in NVC within the low frequency range (0.1 mHz to 2 mHz) as measured using WTC with the full time-scale (or time-frequency) analysis of the three aEEG tracings versus SctO2. The underlying basis of the observed robustness of the WTC-derived NVC to the different aEEG algorithms resides on the fact that WTC features coherence between two sets of time series. By looking at the frequency content of each signal, we can make conclusions on how fast (slow) the signal changes

over time. Information about the frequency content of a signal can be deduced from its frequency spectrum. Some signals change very rapidly as EEG and are therefore mainly associated with high-frequency components. Other signals change very slowly as NIRS; the frequency spectrum of such signal is mainly comprised of a very narrow band of low frequency components. The wavelet measures NVC via oscillations at different time scales via a time-frequency representation. When one wants to compute the interaction between two signals, it is important to define on which time scale the coupling is ought to be computed (the signals are interacting), and the signals have to be matched correspondingly.

Since the NIRS reflects the cardiovascular oscillations which develop in seconds at long-term scale (low frequency activity), the speed of fluctuations is much lower compared to EEG oscillations. This results in down-sampling the 256-Hz aEEG data to a very low frequency around 0.21 Hz that is used for SctO2 data acquisition irrespective of the processing algorithm used. In this process, high frequency components (caused by motion artifacts and other noises) of the aEEG signals are reduced, and low

frequency aspects (related to physiological signals such as neurovascular coupling) are highlighted. Note that the findings were based on the SctO2 device which results in a low sampling frequency of 0.21 Hz.

Of note, caution is indicated in conditions with low NVC as observations in Fig. 2-5 indicate that strong NVC coupling is associated with a smaller variation and/or less effect caused by different aEEG algorithms, and vice versa. These findings therefore need to be replicated in a larger cohort with asphyxia to ensure the validity of this physiological biomarker and its association with long-term clinical outcomes.

2.5. Conclusion

The study demonstrated a good agreement among WTC-based NVC values derived by the three aEEG algorithms regardless of the differences in aEEG tracings. Findings suggest that NVC is a more robust parameter than the automated aEEG patterns, supporting the validation in a large group of newborns with hypoxic ischemic encephalopathy.

Chapter 3

Assessment of Neurovascular Coupling (NVC) in Newborns Using EEG versus amplitude-EEG (aEEG)

3.1. Introduction

Brain function and cerebral oxygenation monitoring in neonatal HIE using multichannel standard EEG with two simplified analysis methods (i.e., amplitude integrated-aEEG and two-channel C3-C4 EEG) and near infrared spectroscopy (NIRS) have been a standard care of practice for decades[10-13]. But till date there is no gold standard method to calculate aEEG[13,14]. New aEEG systems are competitively flooding the market everyday with their innovative and advanced tools to help clinicians assess brain health by the bedside[5]. Lack of a standardized prototype to process aEEG from raw EEG allows developers to innovate the algorithms in a multitude of ways which are often undisclosed and causes differences in the aEEG amplitude margins[5,15]. In general, the algorithms share some common preprocessing steps before conversion of EEG to aEEG. Specifically, a train of EEG signal recorded at the bedside are band-passed from 2-15 Hz using asymmetrical filter to slightly attenuate the dominant delta-wave patterns[16]. The filtered signal then goes through a full wave rectifier and envelope of the rectified signal is extracted. In order to perform NVC, the envelope of the fast-changing EEG signal is down sampled to match the sampling rate of regional NIRS signal. The dynamics of the signal post resampling vary among different algorithms depending on the selection of window length, peak detection, and degree of smoothing filter employed by the algorithms. These differences among algorithms may result in the variability of aEEG tracings with respect to upper and lower margin amplitudes (UMA and LMA, respectively) which affect the clinical display pattern[5,15]. This poses a serious challenge to clinicians who depend on the range of UMA and LMA to assess the severity of HIE. Careful selection of algorithm settings by the clinicians is recommended to minimize the differences in shape and amplitude voltage at the bedside.

The key finding in our prior study[15] highlighted the robustness of NVC based on WTC analysis between aEEG signal and SctO2 in newborns with encephalopathy irrespective of variability in aEEG processing algorithms. The current proof of concept investigation aims to further examine the rigor and consistency of the novel neurovascular wavelet bundle methodology by (1) evaluating the effects of raw EEG recordings on NVC assessment obtained from the same population of infants considered in our prior study, and (2) comparing the variability of WTC-derived metrics derived from raw EEG with that obtained from each of the three aEEG methods previously described. Our null (*Ho*) hypothesis and alternate hypothesis (*Ha*) are designed as:

Ho: Raw EEG can be used instead of aEEG to perform NVC assessment with NIRS-SctO2, for clinical decision making in newborns.

Ha: Raw EEG cannot be used to perform NVC assessment with NIRS-SctO2 in newborns.

Similar NVC assessment between EEG and aEEG can save the clinicians from the hassle of relying on any specific aEEG quantification system for interpretation of HIE severity.

3.2. Materials and methods

3.2.1. Study population and measurement protocol

To test the rigor of NVC assessment in newborns, we selected a convenience sample of eight newborns with HIE (same population of infants considered in our prior study[15]) who had a minimum of twenty hours of simultaneous EEG and NIRS-SctO2 monitoring as a standard of care protocol. Infants had a birthweight of ≥1800 g, were ≥36 weeks of gestation, and admitted to the neonatal intensive care unit at Parkland Hospital, Dallas, TX with evidence of fetal acidosis and encephalopathy. MRI was performed on the infants at a median age of 5 days. Infants had normal MRI outcome and none of these infants had seizures during their recording period.

EEG signals were recorded at a sampling rate of 256 Hz from eight electrodes which were placed on the infant's head at C3, C4, P3, P4, O1, O2, Cz, and Fz locations according to the 10-20 international

system. EEG signals were then amplified and filtered within a frequency band of 0.1-100 Hz. An INVOS spatially resolved NIRS oximeter, consisting of a neonatal probe with a light emitting diode and two distant sensors, were placed on the infant's forehead to record SctO2 at a speed of 0.2 Hz. Both EEG and NIRS-SctO2 were interfaced with a multi-device synchronization platform (Moberg Research, Inc., PA, USA) for simultaneous recording of two modalities and then saved for off-line analysis using MATLAB (Mathworks, Inc.,MA, USA). For this specific study, the time-series information from only the cross cerebral electrode pair C3-C4 (electrodes in central region) is used to perform dynamic wavelet coherence analysis with NIRS-SctO2 in all the neonates[15]. The study was approved by the Institutional Review Board of the University of Texas Southwestern Medical Center and informed consent was obtained from parents of each newborn before enrollment.

3.2.2. Data preprocessing for three methods to acquire aEEG

The raw EEG was converted to amplitude-EEG using three different methods, Method 1 (M1) was derived from the algorithm reported by Zhang and Ding[17]. Method 2 (M2) made use of neonatal EEG analysis toolbox (WU-NEAT) from Washington university, which is an open-source, MATLAB-compatible, clinically validated toolbox to quantify aEEG[18]. Method 3 (M3) extracts aEEG output tracings directly from a commercial synchronization platform using an undisclosed algorithm (CNS Reader, Moberg ICU Solutions, Ambler, PA). Each aEEG derived from the same raw EEG time series using each of M1, M2 and M3, respectively, are marked as SctO2→ $aEEG_{M1}$, SctO2→$aEEG_{M2}$, and SctO2→$aEEG_{M3}$ respectively. Generation of aEEG signals from the same raw EEG signal using these three methods and variability observed among them with respect to aEEG tracings with upper and lower margin amplitudes have been detailed in our recent publication[15]. We demonstrated that regardless of the differences in aEEG tracings the wavelet WTC-based NVC measures using the time-scale analysis between each of the three aEEG tracings and SctO2 showed agreement when derived from three different aEEG algorithms.

3.2.3. Data preprocessing of EEG (fourth method)

The 256-Hz raw-EEG information from C3-C4 channel pair was downloaded from the multi-device synchronization platform (CNS Reader, Moberg Research, Inc., PA, USA). A 2-15 Hz bandpass filter is applied on the raw EEG signal using a 4th order Butterworth filter. Next, the filtered signal was passed through a full wave rectification. The peak-to-peak amplitudes of the 256-Hz rectified signal were measured and sampled at 4.78-s intervals between a common start and end point using cubic spline interpolation algorithm[19] to match the dynamics of SctO2 signal (having a sampling rate of 0.21 Hz) and perform WTC analysis between them. This approach fits the cubic polynomials of 256-Hz signal to the 4.78-s sampled adjacent pairs of points such that the polynomials covering adjacent intervals agree with one another in both slope and curvature at their common endpoint. This method has been referred to as Method 4 (M4) in our study. The preprocessing steps for the output traces derived using M1, M2, M3 and M4 are briefly summarized in Fig. 3-1.

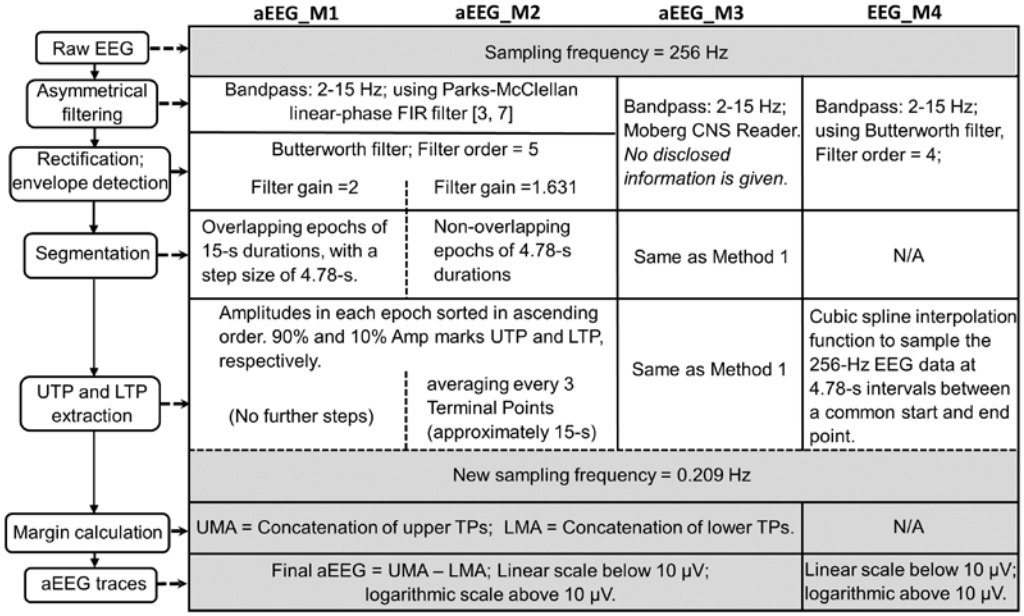

Figure 3-1. Overview of different steps among four data processing algorithms, enroute to obtaining the common sampling rate for aEEG/EEG and NIRS, [Adapted from[15]]; TPs: terminal positions; UTP: upper

terminal positions; LTP: lower terminal positions; UMA: upper margin amplitudes; LMA: lower margin amplitudes.

As an example, Fig. 3-2(a) shows a trace of 5-hour raw EEG signal band passed between 0.1-100 Hz and sampled at 256-Hz from a normal reference control neonate. The y-axis of this figure represents amplitude of pre-processed EEG in micro-volt and is plotted with a linear scale, while x-axis represents time in minute. Fig. 3-2(b) shows three aEEG tracings together with one EEG tracing derived from the original EEG signal shown in Fig. 3-2(a), using M1 (red), M2 (black), M3 (green), and M4 (blue/gray trace) respectively. This example illustrates that even though all four output signals were derived from the same EEG tracing, the amplitude and/or envelop values of the signals vary amongst the methods. Specifically, the variation in the amplitude values of the EEG is clearly differentiable from the envelop values of the three aEEG methods.

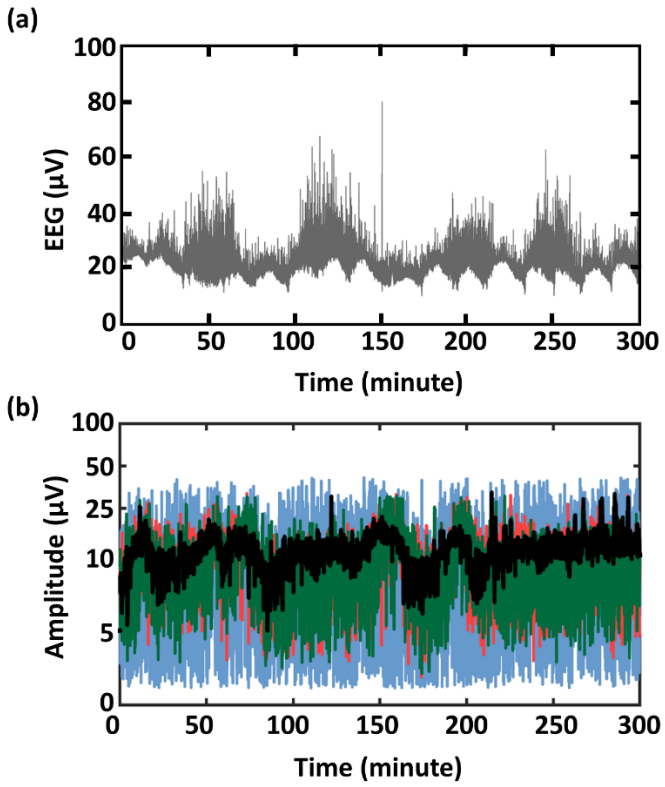

Figure 3-2. (a) An example of 5-hour raw EEG tracings recorded with a 256-Hz sampling frequency. (b) EEG tracing from M4 (blue/gray trace) plotted together with three aEEG tracings obtained using M1 (red), M2 (black), and M3 (green).

3.2.4. Quantification of NVC using the wavelet transform coherence (WTC) statistical methods

We used a MATLAB-based software package[8] to perform wavelet transform coherence (WTC) analysis between the spontaneous oscillations of NIRS-SctO2 and EEG/aEEG signals. WTC is a time-frequency domain analysis, which characterizes the squared cross-wavelet coherence, R^2, between two time series at multiple time scales and over time of any two pre specified variables. The four sets of variables selected for the evaluation of WTC-based NVC in this study are SctO2→ $aEEG_{M1}$, SctO2→$aEEG_{M2}$, SctO2→$aEEG_{M3}$ and SctO2→EEG_{M4}. A 95% confidence interval within each time-scale map identifies statistically significant R^2 values against noise background ($p < 0.05$) by using the Monte Carlo simulation and mark them as statistically significant coherence contours[4,20]. Using a time-scale (equivalent to time-frequency) domain, NVC was assessed by wavelet metric estimation of total pixel number of significant coherence. Specifically, the total pixels (Pix_{total}) was quantified by summing respective pixel numbers across all wavelet time scales within the identified contours (outside of the cone of inference, COI). NVC is represented as the wavelet metric estimation of total pixel number within significant contours. Finally, a coefficient of variation (*COV*) was introduced to evaluate levels of variation between $aEEG_{M1}$, $aEEG_{M2}$, $aEEG_{M3}$ and EEG_{M4} and their effect on WTC-based NVC of each of eight neonates. *COV* was defined as $COV = \frac{SD}{mean\ of\ significant\ coherence\ Pixels}$, where *SD* stands for standard deviation of significant coherence pixels across entire scale from the mean values of significant pixels averaged over those determined with the four algorithms[15]. Statistical analysis to compare agreement between EEG and each of three aEEG methods was performed using Bland Altman curves to detect differences in the estimation of their total pixels count.

3.3. Results

3.3.1. Effect of different processing algorithms on research WTC-derived NVC

The WTC-based time-scale coherence maps obtained from the 8 neonates using four pre-described methods are illustrated in Fig. 3-3, comparing effects of four processing methods on NVC. The figure highlights the consistent time-scale patterns between EEG/aEEG and SctO2 represented in the scale range of 640-10240 s (0.1–1.6 mHz).

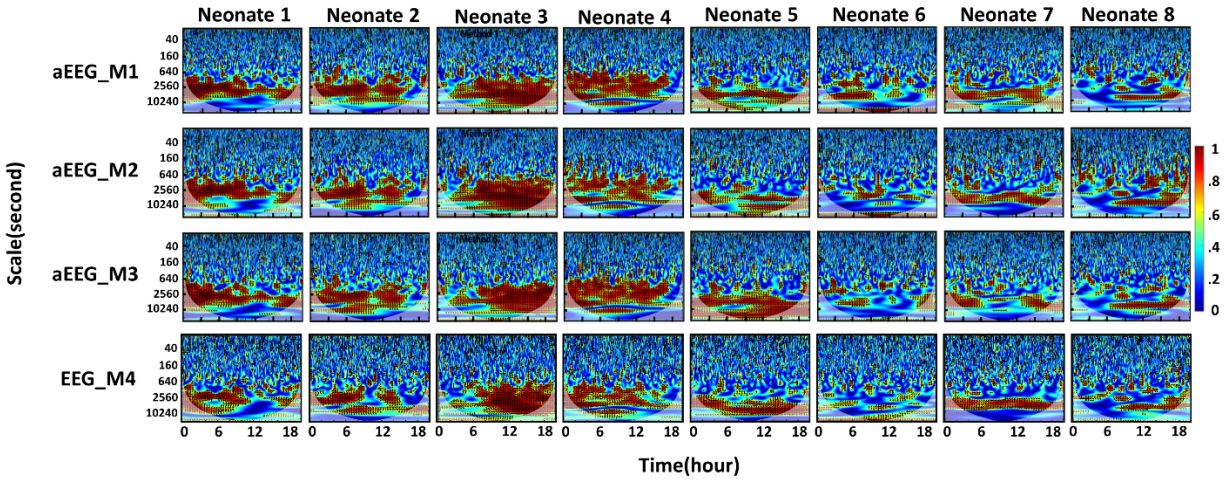

Figure 3-3. Time-scale coherence maps of NVC in the selected cohort. The x-axis represents time in hours, the y-axis represents scale in seconds, and the color scale represents the amplitude of WTC coherence, R^2. The areas with significant NVC ($p<0.05$) are contoured with black lines and filled by red color within the time-scale WTC maps. WTC-based SctO2-aEEG and SctO2-EEG coherence (R^2) are plotted for each one of the 8 neonates (Neonate #: N1-N8). Each vertical column represents the results derived from three aEEG methods and a fourth method employing down-sampled EEG, respectively, highlighting the similarity in NVC pattern for each newborn among $R_{SctO2 \rightarrow aEEG\_M1}$, $R_{SctO2 \rightarrow aEEG\_M2}$, $R_{SctO2 \rightarrow aEEG\_M3}$ and $R_{SctO2 \rightarrow EEG\_M4}$.

The common coherence patterns observed in-between rows #1-3 and among multiple neonates despite large variability in the three aEEG methods (M1, M2 and M3) has been already reported in our previous study. In addition to the results from M1-M3, Fig. 3-3 has included M4-derived time-scale coherence

maps of NVC (the bottom row) to compare the effects of using simple down-sampled EEG on NVC. It is observed that despite the large technical difference in the preprocessing of EEG signal, the WTC-based time-scale coherence maps result derived from a simple down-sampled EEG signal yielded similar results to that obtained from traditional aEEG methods.

3.3.2. Calculation of the total number of pixels within statistically significant contours across entire Scale

Fig. 3-4(a) tabulates the total number of pixels (#pixels_M4) that are significantly coherent between SctO2 and EEG across the entire scale (Pix_{total}) for each of eight neonates alongside the number of pixels identified by three aEEG methods. The corresponding *COV* values between the four processing methods ranges from 6% (Neonate 3) to 16.01% (Neonate 6) for the entire scale.

(a)

	#pixels_M1 (x10⁵)	#pixels_M2 (x10⁵)	#pixels_M3 (x10⁵)	#pixels_M4 (x10⁵)	Mean (x10⁵)	SD (x10⁵)	Coefficient of variation (%)
Neonate 1	5.09	5.12	5.28	4.49	5.00	0.35	7.02
Neonate 2	5.67	5.16	5.19	4.57	5.15	0.45	8.74
Neonate 3	6.62	6.87	6.05	6.17	6.43	0.38	6.00
Neonate 4	6.56	5.93	6.82	5.21	6.13	0.72	11.75
Neonate 5	4.43	4.44	5.35	4.3	4.63	0.48	10.46
Neonate 6	4.18	3.47	3.22	2.89	3.44	0.55	16.01
Neonate 7	4.52	4.86	3.66	4.19	4.31	0.51	11.89
Neonate 8	3.71	4.5	3.42	3.82	3.86	0.46	11.78

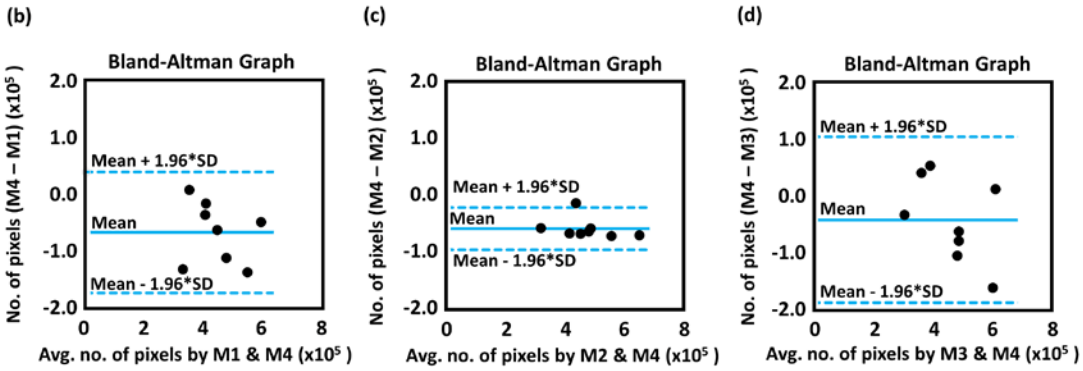

Figure 3-4. (a) Total number of significant coherence pixels derived with M1, M2, M3 and M4 across the entire scale (Pix_{total}) for each of eight neonates. (b-d) Bland-Altman plots to compare WTC-calculated agreements between M4 versus aEEG methods: (b) M1 vs. M4, (c) M2 vs. M4, and (d) M3 vs. M4. The

horizontal upper and lower blue lines mark the limits of agreement, defined as the mean difference ± 1.96 SD.

We utilized Bland-Altman plots to compare the WTC-calculated agreements between total number of significant coherence pixels (#_pixels) derived by M4 across entire wavelet scale range versus #_pixels derived by each of three aEEG methods (M1, M2 and M3), as shown in Fig. 3-4(b–d). Results indicate that the differences in #_pixels are within one standard deviation limit for all neonates regardless of the pair of methodology M1 vs. M4, M2 vs. M4, or M3 vs. M4. This observation implies that despite large signal processing differences with conventional aEEG algorithms, a significant level of agreement/ consistency on WTC-based NVC exists between assessment of SctO2-EEG coherence and assessment of SctO2-aEEG coherence (derived from any of the three aEEG methods) during the entire monitoring period.

3.4. Discussion

In this study, we have established the robustness of the neurovascular wavelet bundle methodology which enables an unprecedented real time analysis of neurovascular coupling non-invasively at the bedside. Key finding highlighted in this study is that NVC assessment based on WTC analysis between an electrophysiological signal and SctO2 in newborns with encephalopathy remains unchanged, irrespective of EEG and aEEG used for data analysis. We hypothesized that raw EEG can be used instead of aEEG to perform NVC assessment with NIRS-SctO2, for clinical decision making in newborns. Based on the statistical analysis, our null hypothesis cannot be rejected, and raw EEG with a one-step resampling can be used to perform NVC assessment with NIRS-SctO2 instead of hovering through several unspecific data processing pipelines to obtain aEEG.

The multitude of differences between the aEEG algorithms has been discussed in our previous study and careful selection of the algorithm settings was recommended at the bedside, as these differences could potentially impact the clinical decision makings by the clinicians[5,15]. Specifically, since the decision

to put a neonate into hypothermia treatment depends highly on the aEEG margin classification from the automated tools[21,22], much caution is needed. However, this study demonstrates that the novel WTC-based NVC assessment in newborns remains unaffected even when performed directly on raw EEG. This adds a feather to the significance of this study by confirming that NVC can also be performed directly on the down sampled EEG using wavelet analysis, without the headache of having to choose between anyone of the many available aEEG algorithms, if the clinicians wishes to.

The root cause behind the broader bandwidth of output from M4 in Fig. 3-2 owes to large physiological variability of the raw EEG signal followed by a simple bandpass filter, whereas, output tracings from aEEG algorithms pass through several low pass filters that results in envelope extraction followed by few layers of data smoothing. This eventually leads to a narrower bandwidth of the output signals from M1, M2 and M3, compared to simple one-step down-sampling in M4.

aEEG has traditionally been applied to surveil the brain development and screen cerebral pathologies by evaluating the background pattern and sleep-awake cycles in Neonatal Encephalopathy[23]. The digital calculation of aEEG was first described by Maynard et al.[16] and a lot of studies have thereafter published normal and abnormal amplitude margin ranges for preterm and term infants[13,24,25]. These output amplitude tracings are displayed in a semilogarithmic (linear 0–10 μV, logarithmic 10–100 μV) and time-compressed (6 cm/h) format[16], following some general procedure of aEEG data processing. Although the calculation of these amplitude margins (LMA and UMA) vary between different aEEG devices, for the sake of convenience clinicians still like to look at the lower, upper and bandwidth of the margin amplitudes to describe the background patterns of the neonates at the bedside. Any divergence from such pipelines will reflect on the bandwidth of the output signals which when plotted in semilogarithmic scale may create confusion in clinician's mind.

3.5. Conclusion

Our findings confirm the robustness of NVC wavelet analysis related to HIE irrespective of EEG or aEEG algorithms used. This approach reduces complexities more in the post processing steps in signal-processing domain that can potentially enhance the translational rigor of real time physiological biomarkers in the future. But for the immediate convenience of clinicians by the routine bedside, use of aEEG is better recommended over EEG.

Chapter 4

Novel Wavelet-Based Neurovascular Coupling (NVC) Approach to Predict Brain Abnormalities of Encephalopathy Newborns in The First Day of Life

4.1. Introduction

Birth asphyxia remains a serious clinical burden that affects millions of newborns worldwide every year and hypoxic–ischemic encephalopathy (HIE) remains as an important cause of neuro-developmental impairment, long-term disability, and death in these encephalopathic newborns[26,27]. However, successful initiation of neuroprotective therapy, such as hypothermia within 6-h of birth, has proven to improve outcome in HIE by reducing risk of cerebral palsy and significant disability in neonates with moderate and severe HIE[28,29]. Therapeutic hypothermia (TH), continued for a period of 72-h, aims at slowing down the body's metabolic rate and provides more time for neuronal cells to recover from neurological damage[30]. During TH, acquiring amplitude-integrated electroencephalography (aEEG), which measures aggregated neuronal activity, and near infrared spectroscopy (NIRS)-based cerebral tissue oxygen saturation (SctO2), a surrogate of cerebral blood flow (CBF), have been a standard care of practice in neonatal encephalopathy (NE) for decades to monitor evolving encephalopathy and to predict brain injury or neurodevelopmental outcome[1,31-33]. After the completion of TH, rewarming and normothermia, a brain magnetic resonance imaging (MRI) is obtained on all newborns prior to discharge for an evidence of neurological injury.

Although bedside monitoring of aEEG and NIRS-SctO2 remains as important tools to study the effect of TH on outcomes, predictive abilities of aEEG following the introduction of TH in the first day of life have been reported to provide false positive values and become more reliable after 24-h[11,34,35]. Various factors, such as TH initiation time, extent and time course of injury following TH, may impact the predictive characteristics of aEEG which makes the data unreliable in the first 24-h[35,36]. Although high values of lower margin amplitude (LMA) and mean aEEG voltage at 24 to 48-h are found to be associated

with good neurological outcome[37], early prognostication based on visual interpretation of background /voltage pattern and sleep-awake cycle from first 24-h aEEG may be challenging[34]. On the other hand, studies conducted on cerebral NIRS monitoring in newborns with HIE revealed a significant difference in the cerebral oxygenation from birth till 12-hours of life (HOL) between groups with evidence and absence of cerebral injury shown on MRI[38]. Cerebral oxygenation in encephalopathy neonates drops in the first 4-6 HOL following injury and recovers by 18-20 HOL [38]. However, a study by Shellhaas et al. found no definite relationship between cerebral oxygenation and neurodevelopmental outcome at 18 months[39]. Combined clinical neuromonitoring using NIRS and aEEG monitoring is feasible, but there is a critical need to develop reliable and powerful real time physiological biomarkers so as to aid in stratification of encephalopathy severity and predicting a brain injury in newborns in the first day of life.

So far, no studies have been reported that can predict brain injury in the neonates in the very first day of life. Chalak et al. reported that wavelet measures of NVC in the first 72 HOL are associated with long-term outcomes 18-24 months following NE, with and without TH[4]. The study was performed between eight neonates with moderate to severe encephalopathy who received hypothermia and two with no encephalopathy who did not meet criteria for cooling and served as references. While TH has been a standard care of practice in neonates with moderate and severe HIE[40-42], infants with mild HIE are excluded from TH due to a perceived low risk of death or major disability based on data from the pre-hypothermia era[22,43,44]. However, recent studies have reported that 52% of infants, who were initially identified with mild HIE in the first 6-h after birth and did not receive TH, later came back with short-term abnormalities[45,46], questioning the conventional definition of mild HIE within 6-h.

The current proof of concept investigation specifically targets the feasibility of using WTC-based-NVC as a physiological biomarker to predict the presence of brain injuries in newborns in the very first day of life. The study cohort includes neonates with mild to severe encephalopathy, with subsets of normal and abnormal MRI injury candidates in each group. The encephalopathy of these neonates was evaluated based on a neurological examination (Total Sarnat Score, a.k.a. TSS) performed in the first 6-h of life. Therefore, the important focus of this paper is to investigate if NVC in the first day of life can

identify the subset of neonates, regardless of their initial encephalopathy grade, who are at a higher risk of developing abnormality at a later phase.

4.2. Materials and methods

4.2.1. Study population and measurement protocol

This study included a total of 36 newborns with evidence of fetal metabolic acidosis and encephalopathy within the first six hours of birth who were evaluated and screened during the one-year study period between March 2018 to February 2019. These infants had a birthweight of ≥1800 g, were ≥36 weeks of gestation, and admitted to intensive care unit at Parkland Hospital, Dallas, TX. Neuromonitoring was initiated at 12 +/- 2 hours of birth and continued for a duration of at least 20 hours. Electroencephalogram (EEG) and regional cerebral tissue oxygen saturation (SctO2) by near infrared spectroscopy (NIRS-SctO2) of all neonates were simultaneously recorded during the entire course of monitoring, which made it feasible to perform dynamic wavelet coherence analysis between the signals. The study was approved by the Institutional Review Board of the University of Texas Southwestern Medical Center and informed consent was obtained from parents of each newborn before enrollment.

4.2.2. Encephalopathy severity classification

The encephalopathy severity of a neonate is graded based on a neurological exam performed within the first six hours of life known as Total sarnat score (TSS). TSS is used to assess the status of a neonate following birth asphyxia by taking into account few aspects that are associated with clinical dysfunction such as their level of consciousness, spontaneous activity, posture, tone, primitive reflexes (suck, moro) and autonomic system (pupils, heart rate, respiration)[46,47]. In the scoring system, a score of 0 is considered normal and the maximum score of 22 signifies the worst possible status of HIE. From the selected sample of thirty-six neonates, 15 infants with TSS score between 1–10 are considered to have ‘mild’ HIE (aka. Sarnat stage 1) and 14 neonates have ‘moderate’ HIE (with score of 11–14; aka Sarnat stage 2). The three of the remaining 7 neonates were quantified into ‘severe’ HIE group (TSS >15) and four neonates escalated from mild to moderate, the scope of this study is restricted to mild (n=15) and moderate (n=14)

encephalopathy groups only. Post scoring, the neonates with stage 2 sarnat scores (moderate encephalopathy) are introduced to TH, which is a standard of care for infants ≥36 weeks gestational age with moderate-to-severe hypoxic-ischemic encephalopathy. While hypothermia provides neuroprotection via reduction in cerebral metabolism as well as cerebral blood flow[30], a continuous brain monitoring using EEG and NIRS-SctO2 at the background is used to assess brain health of these neonates for a duration of at least twenty hours.

4.2.3. Neuroimaging assessments

A 3-Tesla MRI (Philips Healthcare Systems, TX) was performed on all neonates at a median age of 5 days age for evidence of neurological abnormalities and injuries. MRI findings were scored for abnormalities by an experienced pediatric neuro-radiologist based on National Institute of Child Health and Human Development (NICHD) classification[48,49]. The recruited cohort was divided into two groups, group 1 comprised of 26 neonates having normal MRI outcome and group 2 comprised of 10 neonates with abnormal MRI outcome who had mostly white matter injury and watershed infarcts.

4.2.4. EEG and NIRS data preprocessing

EEG data were acquired from eight electrodes placed on newborn's scalp at C3, C4, P3, P4, O1, O2, Cz, and Fz locations, according to the 10-20 international system. EEG signals were recorded at a sampling rate of 256 Hz and then amplified and filtered within a frequency band of 0.1-100 Hz. Regional SctO2 was measured on the neonate's forehead using an INVOS™ 4100–5100 oximetry (Somanetics, Troy, MI) and a neonatal sensor, at a sampling rate of 0.21 Hz. Both EEG and NIRS-SctO2 signals were interfaced with a multi-device synchronization platform (Moberg Research, Inc., PA, USA) for simultaneous recording of two modalities and then saved for off-line analysis using MATLAB (Mathworks, Inc., MA, USA). For this specific study, the time-series information from cross-cerebral electrode pair C3-C4 (electrodes in central region) is used for data analysis of all the neonates. The EEG data from C3-C4 channel pair was first passed through an asymmetric band-pass filter (Parks-McClellan linear-phase FIR filter), strongly attenuating the signal below 2 Hz and above 15 Hz and converted to amplitude-EEG

(aEEG) using Washington University-Neonatal EEG Analysis Toolbox (WU-NEAT), which is demonstrated as Method 2[15] in our previous study. Both the SctO2 and aEEG data were inspected to identify artifacts, which were removed by linear interpolation between neighboring data points, followed by a second-order polynomial de-trending to remove the slow drifts of each time series.

4.2.5. Wavelet coherence analysis

We used a MATLAB-based software package to perform wavelet transform coherence (WTC) analysis between the spontaneous oscillations of artifact-free NIRS-SctO2 and aEEG signals[8] as we recently published in neonatal encephalopathy[15,20,50]. WTC is a time-frequency domain analysis, which characterizes the squared cross-wavelet coherence, R^2, and relative phase, $\Delta\phi$, between two time series at multiple time scales and over the entire time duration, without a prior assumptions of linearity and stationarity. R^2 can be conceptualized as a localized correlation coefficient between these two signals in time-frequency domain which can range anywhere between 0 and 1. The statistical significance of R^2 is estimated based on Monte Carlo simulation which uses 95% confidence interval to identify the R^2 regions that are statistically significant against simulated background noise ($p < 0.05$)[51]. All the pixels who had statistically significant coherence values are marked as black contours within the time-scale map. Using a time-scale (equivalent to time-frequency) domain, NVC was assessed by wavelet metric estimation of percentage of total pixel number of significant coherence. Specifically, the number of significant pixels (Pix_{total}) was quantified by summing pixel numbers across all wavelet time scales only within the identified contours (outside of the cone of inference, COI). Next, Pix_{total} is divided by the total number of pixels, both in and outside of black contours within the wavelet time-scale map to represent the NVC in percentage. The percentage of significant coherence between SctO2 and aEEG is quantified across all phase ranges.

4.3. Results

The top panel (a-c) and bottom panel (d-f) of Fig. 4-1 show examples of aEEG (represented in µV) and SctO2 (represented in %) tracings, continuous wavelet transformation of corresponding signals and time-scale maps of NVC in the selected cohort of two neonates, with normal (neonate #17) and abnormal (neonate #28) MRI outcome, respectively. The y-axes of all the time-scale maps represents frequency/scale in minutes, and x-axes represents time in hour. The color scale of (b, c) and (c, f) represents the amplitude of power after CWT and amplitude of WTC coherence, R^2, respectively. The areas with significant NVC ($p < 0.05$) in (c, f) are contoured with black lines and filled by red color within the time-scale WTC maps.

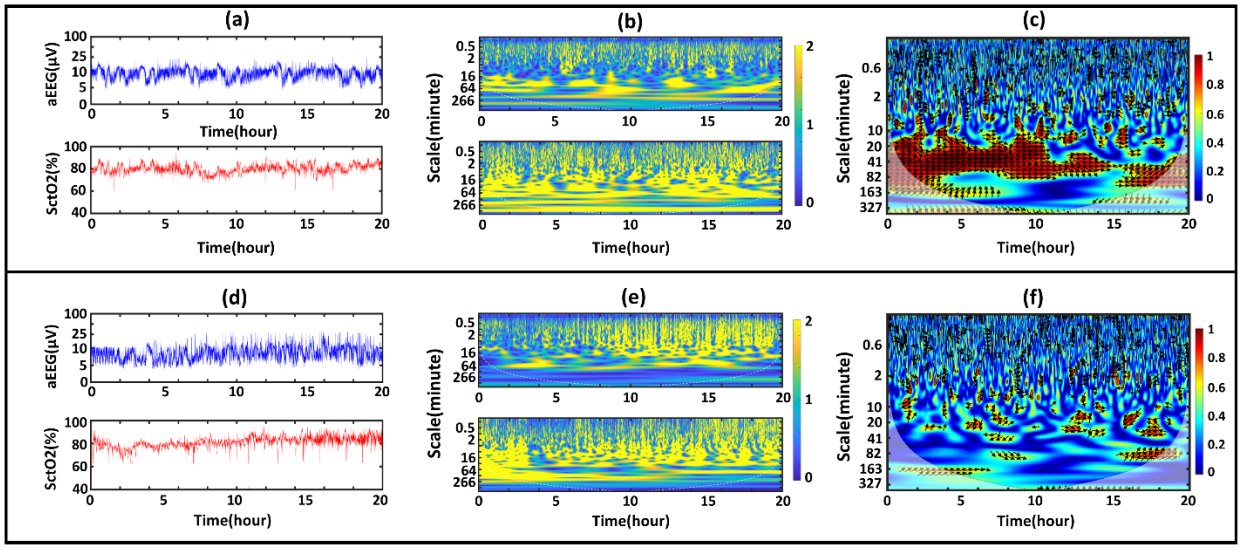

Figure 4-1. Top and bottom panels illustrate examples of graphs from two neonates with normal and abnormal MRI, respectively. Left (a, d): examples of simultaneously recorded 20-h aEEG (in µV) and SctO2 (in %) tracings from two selected neonates, each sampled at 0.21-Hz. Middle (b, e): Wavelet transformation of the corresponding tracings from (a, d), where y-axis represents scale in minute and the color scale represents the amplitude of power after CWT. Right (c, f): Time-scale coherence maps of NVC in the selected cohort, y-axis represents scale in minute, and the color scale represents the amplitude of WTC coherence, R^2. The x-axis of all panels represents time in hour.

Fig. 4-1(a) shows 20-h simultaneous recordings of aEEG and SctO2 tracings from a neonate with normal MRI outcome. The neonate had an early indication of normal sleep-awake cycle and continuous voltage range throughout the recording, with upper and lower aEEG margins >10μV and >5μV respectively, the mean SctO2 recorded across 20-h is 79.86%. Panel 4-1(d) shows aEEG and SctO2 tracings from a neonate with abnormal MRI outcome who had white matter injury in a few subcortical regions accompanied by subtle diffused restriction. The neonate indicates gradual increase in the amplitude margin range with inconsistent sleep-awake cycle, and oxygen saturation level after 10-h with mean SctO2 was recorded at 81%.

Next, we performed time-frequency analysis of the aEEG and SctO2 signals using continuous wavelet transform (CWT) and analytic Morlet wavelet[8]. The corresponding time-frequency spectrograms of the two neonates are shown in Fig. 4-1(b, e), where the x-axis represents time in hour, the y-axis represents scale in minute, and the color scale represents the amplitude of power after CWT. The variability in the power distribution of signals between normal and abnormal cases are evident. The magnitudes of power obtained from aEEG and SctO2 signals of normal neonate are evenly distributed across time (Fig. 4-1b), whereas, time-frequency representation of each of these signals coming from abnormal neonate marks sudden increase in the signal power post 10-h, as observed in Fig. 4-1(e).

Furthermore, the WTC-based time-scale coherence maps of NVC, R^2, obtained from the neonates with normal and abnormal MRI outcome, respectively, are illustrated in Fig. 4-1(c, f). Although it is difficult to interpret any visual difference between neonates by looking at their aEEG and SctO2 traces, however, the neonate with normal MRI outcome have notably high NVC coherence, observed specifically in the scale range of 16-150-minute, compared to low coherence observed in the neonate having with MRI abnormalities.

4.3.1. Wavelet findings

4.3.1.1. Normal and abnormal MRI outcome group

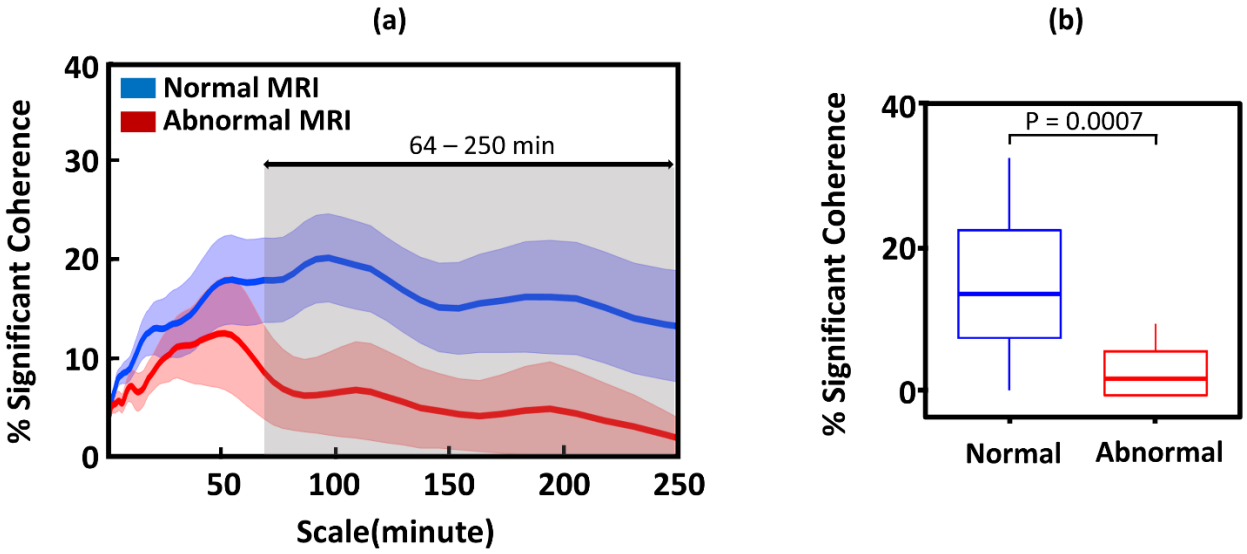

Figure 4-2. (a) Mean significant SctO2→ aEEG coherence from newborns quantified in: (1) normal MRI outcome group (n = 26) shown in blue, and (2) abnormal MRI outcome group (n = 10), shown in red, based on global MRI scoring. Significant differences between normal vs. abnormal groups ($p < 0.05$) was observed in the selected wavelet scale range of 64–250 min. Fig. 4-2(b) shows statistically significant coherence in the selected wavelet scale range of 64–250 min. Boxplot (median, 25% and 75% percentiles) representation for the % NVC coherence across all phases showed 95% significance with ($p = 0.0007$) by Exact Wilcoxon rank sum test.

At group level, Fig. 4-2(a) shows the percentage of mean significant coherence between SctO2 and aEEG identified across 26 normal and 10 abnormal MRI neonates, color coded in blue and red, respectively. The blue and red shaded regions in the background represent the standard error of coherence for corresponding normal and abnormal group, respectively. Wavelet based SctO2-aEEG coherence showed higher NVC in neonates with normal MRI outcome, calculated across all phases. A clear visual separation between the SctO2-aEEG coherence of two groups is observed in the wavelet scale range of 64-250 minute and is selected for statistical analysis.

According to the exact Wilcoxon Rank Sum test performed in-between groups in Fig. 4-2(b), significant coherence ($p < 0.001$) between SctO2 and aEEG was identified by the wavelet analysis in the

wavelet scale of 64–250 minutes equivalent to a very low-frequency (VLF) range of 0.00006–0.0002 Hz. This figure highlights that the phenomenon of NVC can be used as a physiological biomarker to accurately predict any possibilities of MRI injuries in the encephalopathy neonates in the first day of life.

4.3.1.2. Newborns quantified in (a) 'mild' HIE, having normal and abnormal MRI outcome, (b) 'moderate' HIE, having normal and abnormal MRI outcome

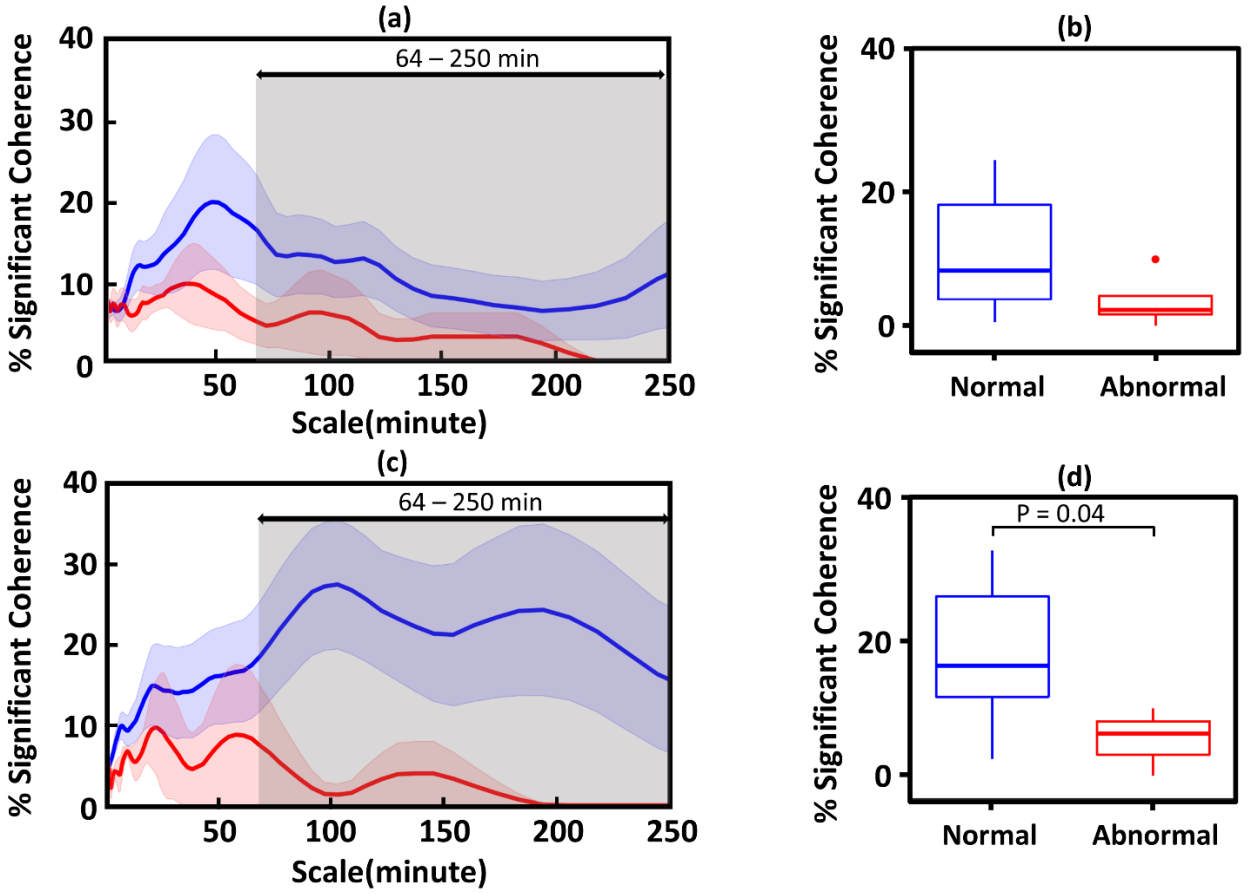

Figure 4-3. Mean significant SctO2→ aEEG coherence from newborns quantified in (a) 'mild' HIE, having normal (n=11, shown in blue) and abnormal (n=4, shown in red) MRI outcome, (c) 'moderate' HIE, having normal (n=12, shown in blue) and abnormal (n=2, shown in red) MRI outcome. The solid lines represent mean coherence of each group and shaded region at the background represents standard error, color-coded of respective groups. Figures on the right (b and d) highlights statistical difference between SctO2→ aEEG coherence of normal vs. abnormal group in the selected

wavelet scale range of 64–250 minute, separately under the label of ‘mild’ HIE (Fig. 4-3b) and ‘moderate’ HIE (Fig. 4-3d).

Fig. 4-3 shows further quantification of neonates with normal (represented in blue) and abnormal (represented in red) MRI, under subsets of ‘mild’ (top panel) and ‘moderate’ encephalopathy (bottom panel). It provides a bird’s eye visual concept of the fact that MRI exam on day 5 or 6 can identify/separate mild and moderate HIE neonates in the first day of life. Although statistical evidence is a subject to further exploration on larger cohort and beyond the scope of this study.

In group level, the neonates with normal MRI outcome in both ‘mild’ (n=11) and ‘moderate’ (n=12) encephalopathy group indicated a higher percent of coherence between SctO2 and aEEG. On the contrary, neonates with abnormal MRI injuries, irrespective of their original encephalopathy grade (based on TSS) as ‘mild’ (n=4) or moderate’ (n=2), have a common phenotype which is low NVC. These findings are similar to that observed in Fig. 4-2.

Within each HIE subset of mild and moderate, we performed statistical analysis between MRI groups in similar wavelet scale range of 64-250 minute to maintain consistency. Statistically significant SctO2→ aEEG coherence ($p < 0.04$) was identified between the normal and abnormal neonates with ‘moderate’ encephalopathy. Although no statistical difference is observed between the coherence of normal and abnormal neonates in mild encephalopathy group, however, both the statistical plots provides a good visual. Overall, the phenomenon of NVC in the first day of life allowed us to identify the MRI abnormalities irrespective of their original classification as mild or moderate.

4.3.2. TSS relationship with percent NVC in light of their association with predicting abnormalities in the first day of life

Based on TSS examination, neonates are quantified into mild and moderate encephalopathy groups within the first six hours life[46]. However, despite having normal scores some mild neonates can still develop MRI-shown brain injuries (n=4 in our study) that can be identified by MRI exam on day 5 or 6[52]. On contrary, majority of moderate encephalopathy neonates with abnormal TSS score ended up showing

no sign of MRI-shown injuries at all. Chalak et. al proposed that TSS of 5 when performed at <6 HOL shows good accuracy to predict higher risk of developing disability at a later stage and indicates a higher encephalopathy burden[53]. In this study, we compared the predictive values of TSS with the percentage of SctO2-aEEG coherence derived using WTC-based-NVC as two biomarkers to identify the neonates with normal and abnormal MRI.

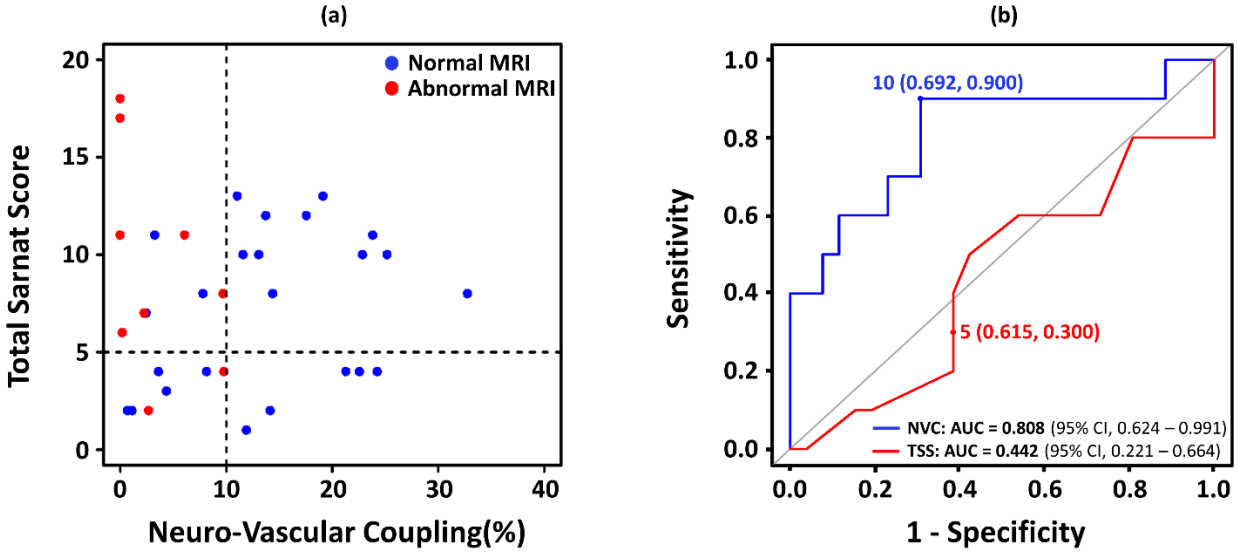

Figure 4-4. (a) TSS relationship with percent NVC in light of their association with predicting abnormalities in the first day of life. (b) Receiver operating characteristic (ROC) curves for TSS and NVC. TSS of 5 is regarded as the safe margin to identify neonates with a higher risk of developing abnormality. NVC is calculated using wavelet transform coherence between dynamic oscillations of SctO2 and aEEG. AUC indicates area under the ROC curve compared to line of non-significance in grey.

Fig. 4-4(a) provides a good visualization of the relationship between TSS and percent NVC with predicting potential for abnormalities in the first day of life, based on MRI results taken 5-6 days after birth. A horizontal dotted line at TSS=5 highlights the empirical TSS boundary to identify neonates with a higher risk of developing abnormality. A vertical dotted line at 10% marks WTC-based NVC decision boundary to identify neonates with abnormalities. In Fig. 4-4(b) receiver operating characteristic (ROC) curves were plotted for TSS (represented in red) and NVC (represented in blue). For the TSS curve, Area

Under Curve (AUC) was 0.442, Sensitivity was 61.5%, Specificity was 30%, Positive Predictive Value (PPV) was 75% and Negative Predictive Value (NPV) was 31%. For the NVC curve, AUC was 0.808. There was a tendency for better predictive capacity of abnormality in regard to NVC (Sensitivity 69%, Specificity 90%, PPV 94% and NPV 52%).

Overall, Fig. 4-4 highlights that 10% NVC has a receiver area under the curve that has the highest sensitivity and specificity for identifying MRI-shown abnormalities, compared to TSS of 5. As a result, our preliminary results suggest that although TSS is a better predictor for neurodevelopmental outcome at <6 HOL, however, it loses the debate to the novel neurovascular wavelet bundle methodology which in the first day of life proved to more efficiently identify the neonates who might potentially be in a risk of developing MRI injuries days later.

4.4. Discussion

This proof of concept study demonstrated the feasibility of using dynamic wavelet transform coherence analysis to assess neurovascular coupling (NVC) by the bedside in the first day of life. Preliminary results suggest that the phenomenon of NVC if performed within the first day of life can successfully predict possibilities of MRI injuries that may develop in later period in the newborns despite of their original label as mild or moderate. The key findings of this study are 1) % NVC is higher for normal MRI group compared to abnormal group in the time scale 16-250 minutes irrespective of their initial encephalopathy grade. 2) There is no statistical difference in % NVC between normal and abnormal MRI group in mild encephalopathy group. 3) In the moderate encephalopathy group, % NVC in normal group is higher than the abnormal MRI group 4) Percentage NVC of 10 has a significant optimal cutoff to distinguish normal and abnormal MRI groups.

Based on the studies conducted prior to hypothermia it often became challenging to clinically discern between mild and moderate NE severity within a short therapeutic window after birth. There has been an increase in the evidence of cognitive impairment in a subset of 30–50% of “mild NE” cases at 18-24 months, who are not recognized during postnatal classification and hence not included in early

neuroprotection trials[45,46]. Therefore, an important focus of research is to recognize this conundrum[54-56] and look for better physiological biomarker that will allow early and accurate identification of infants at risk for adverse outcomes who might benefit from targeted treatments. Since survival and neuro-developmental impairment at 2 years of age is primarily considered as the gold standard for safe assessment of outcome in neonatal studies[57], several studies have been conducted over last decades in search for early prognostication and risk stratification abilities of biomarkers such as MRI and TSS with reference to outcome of disability at 18-24 months of age[52,53,58,59].

Neuroimaging methods such as MRI describes essential links between the brain and behavioral changes in neonates. MRI performed on the HIE neonates at an age of 5 ± 1 days generally describes the brain injury as either white matter (WM) injury extending to the cortical areas or deep gray nuclei injury in the basal ganglia or thalamus (BGT), or involvement in both areas[60-63]. In newborns, evidence of neurological abnormalities and injuries in these areas are associated with cognitive delays and motor impairment[64-66]. A recent study examined the association between prognostic ability of MRI in the assessment of brain injury and neurodevelopmental outcome at 18-24 months and reported that abnormal MRI assessment following period of TH appears to be a biomarker of disability at 2 years outcome, whereas, a normal MRI was predictive of normal outcome[58].

Since the neurodevelopmental outcome at 18-24 month age of the 36 neonates recruited for this study is not yet available, this study considered MRI classification of the neonates as the gold standard and evaluated the predictive abilities of WTC-based NVC between their SctO2 and aEEG signals to predict brain injuries in the first day of life. The new findings of this study suggests that percent of neurovascular coupling using wavelet transform coherence analysis can be used as potential physiological biomarker that can forecast any possible abnormalities in MRI outcome based on neurovascular function in the very first day of life itself. This can better help the clinicians to be able to quickly assess severity of HIE on the bedside life and quickly provide appropriate and timely interventions to prevent permanent injury of the neonatal brain.

To further demonstrate the rigor of wavelet methodology in predicting the neuro-developmental outcome, we compared the ROC curves of TSS and wavelet metrics derived from NVC. In the Prospective Research for Infants with Mild Encephalopathy (PRIME) study, Chalak et. al proposed a new scoring system that is specifically designed to identify infants ≥ 36 weeks of age with encephalopathy who do not meet the current cooling criteria (a range of 1-10) but indicates a higher risk of developing disability at a later stage[53]. The study correlated score from standardized neurologic examination performed at <6 HOL with the neurodevelopmental outcome at 18-22 months graded using the NICHD criteria[67,68]. The study concluded that a TSS of 5 when performed at < 6 HOL showed good accuracy to predict disability and indicates a higher encephalopathy burden. While such a scoring approach still awaits validation and replication in larger cohorts, we made an attempt to compare the predictive values of TSS with the percentage of SctO2-aEEG coherence derived using WTC-based-NVC in the entire HIE cohort (Fig. 4-4). Our preliminary results suggest that although total Sarnat score is a better predictor for neurodevelopmental outcome at <6 h of age, however, novel neurovascular wavelet bundle methodology proved to more accurately classify neonates with and without MRI injuries in the first day of life.

This new wavelet bundle approach once validated in larger cohort and their 2-year neurodevelopmental outcome promises to significantly impact the early NE stratification and prediction of abnormalities. The ability to prospectively monitor the global neurovascular unit functions in real time, via novel approaches as delineated in this study, could in the future provide a paradigm shift to the field of neonatal neuro-critical care and improve the selection of candidates in neuroprotection studies.

4.5. Conclusion

This proof of concept study demonstrated the feasibility of using dynamic wavelet transform coherence analysis to assess neurovascular coupling (NVC) by the bedside in the first day of life. Preliminary results suggest that quantification of NVC being performed within the first day of life can successfully predict possibilities of MRI-shown brain injuries that may develop 5-6 days after birth in the newborns despite of their original stages as mild or moderate HIE. Validation on a larger cohort will be taken in future studies.

Chapter 5

Assessment of the scale-dependent percentage of wavelet-based significant in-phase coherence to stratify the spectrum of encephalopathy severity between mild, moderate, and severe HIE neonates in the first day of life

5.1. Introduction

This study is an extension of chapter 4. The encephalopathy of these neonates was evaluated based on a neurological examination (Total Sarnat Score, a.k.a. TSS) performed in the first 6-h of life. While TH has been a standard care of practice in neonates with moderate and severe HIE[40-42], infants with mild HIE are excluded from TH due to a perceived low risk of death or major disability based on data from the pre-hypothermia era[22,43,44]. However recent studies have reported that 52% of infants, who were initially identified with mild HIE in the first 6-h after birth and did not receive TH, later came back with short-term abnormalities[45,46], questioning the conventional definition of mild HIE within 6-h. Therefore, the important focus of this chapter is to investigate if NVC using wavelet analysis can be used as a real-time physiological biomarker, instead of conventional sarnat scoring, that can clinically discern the spectrum of encephalopathy severity among mild, moderate and severe HIE neonates in the first day of life. The sarnat score classification of the neonates performed within first 6 hours of birth is considered as the gold standard, based on which this study divided the pool of 36 neonates into four encephalopathy groups, namely 'Mild' (n=15), 'Mild_to_Moderate' (n=4), 'Moderate' (n=14), and 'Severe' (n=15). WTC-based NVC was performed on all the neonates between their SctO2 and aEEG signals, recorded in the first day of life and statistical analysis was performed for each of the following groups, 1. Mild and Moderate, 2. Mild, Moderate and Mild_to_Moderate, 3. Mild, Moderate and Severe.

5.2. Materials and methods

5.2.1. Study population and their severity classification

The same pool of 36 neonates from the MRI study who were admitted to intensive care unit at Parkland hospital, Dallas between March, 2018 to Feb,2019, are selected for this study, their encephalopathy severity is graded based on neurological exam performed within first 6 hours of life known as Thompson sarnat score. In the scoring system, a score of 0 is normal and the maximum score is 22 which signifies the worst possible status of HIE. 15 infants with score between 1–10 are considered to have 'mild' HIE (Sarnat stage 1), 14 neonates have 'moderate' HIE (with score of 11–14 - Sarnat stage 2) and 3 neonates are categorized in the 'severe' HIE group (with score of 15–22 - Sarnat stage 3). 4 neonates who were initially classified into mild encephalopathy group based on clinical sarnat examination within 6 hours of birth, later showed seizure activity which qualified them to receive therapeutic hypothermia. The seizure activity is most likely a result of an evolving brain injury or worsening encephalopathy, and since these 4 neonates escaladed from mild HIE to moderate, they were considered as 'Mild-to-Moderate' category. Post scoring, the neonates with stage 2 and 3 sarnat scores (moderate and severe encephalopathy respectively) are introduced to hypothermic therapy and while hypothermia provides neuroprotection via reduction in cerebral metabolism as well as cerebral blood flow, a continuous brain monitoring using aEEG and NIRS-SctO2 at the background is used to assess brain health.

5.2.2. Neuroimaging assessments and EEG and NIRS data preprocessing

The procedures were taken in the same way as those given in Sections 4.2.3. and 4.2.4.

5.2.3. Wavelet coherence analysis

I used a MATLAB-based software package to perform wavelet transform coherence (WTC) analysis[8] between the spontaneous oscillations of NIRS-SctO2 and aEEG. Details of this method has been described in section 4.2.5. In this study, WTC-based NVC is represented as the percentage of significant coherence, P(I), between the SctO2 and aEEG oscillations, within the selected phase range of interest (in-phase; range: $\Delta\varphi=0\pm\pi/4$). Specifically, the percent of significant mean in-phase coherence, at each wavelet scale, $P(I)_{scale}$, was calculated for all the neonates, which is quantified as the percentage of time during which the SctO2→ aEEG coherence is statistically significant within the in-phase range and at a certain wavelet scale. Wilcoxon rank sum test is performed on P(I) at each wavelet scale between

neonates of two groups under consideration, and scales which indicated statistically significant difference in mean P(I) between the two groups are subsequently marked. The scale range having the longest chain of scales with statistical significance in P(I) is considered as region of interest (ROI). NVC within ROI WTC time-scale map is quantified by dividing the total pixel number of significant in-phase coherences, $P(I)_{ROI}$, by the total number of pixels outside of the cone of inference, COI), but within ROI for each neonate.

5.3. Results

5.3.1. Investigation of upper and lower range of amplitude aEEG margins

The upper and lower margins of the aEEG shape the top and bottom envelopes of the tracing, reflecting the maximum/minimum peak-to-peak amplitudes of the EEG signals, as shown in panel Fig. 5-1(a). Upper and lower representative aEEG margins were obtained by serial concatenation of all upper and lower terminal points, respectively, using WU-NEAT algorithm[6]. For each neonate, the upper and lower margin amplitude, abbreviated as UMA and LMA respectively, was quantified as the mean of upper and lower representative aEEG margins, respectively, over a duration of 20 hour. Fig. 5-1(b) indicates a gradual decrease in the UMA range of neonates with the increase in their severity of encephalopathy. The neonates with 'mild' encephalopathy are observed to have a normal/continuous amplitude with lower margin >5 μV and upper margin >10 μV, while neonates with 'severe' encephalopathy recorded suppressed amplitude having a mean lower margin <5 μV and upper margin <10 μV. Also, the 'severe' encephalopathy group attained a higher percentage of mean tissue oxygen saturation compared to 'mild' and 'moderate' group. All these results are consistent with previous literature findings[69] and confirm the overall behavioral feature of encephalopathy groups, classified by manual sarnat scoring.

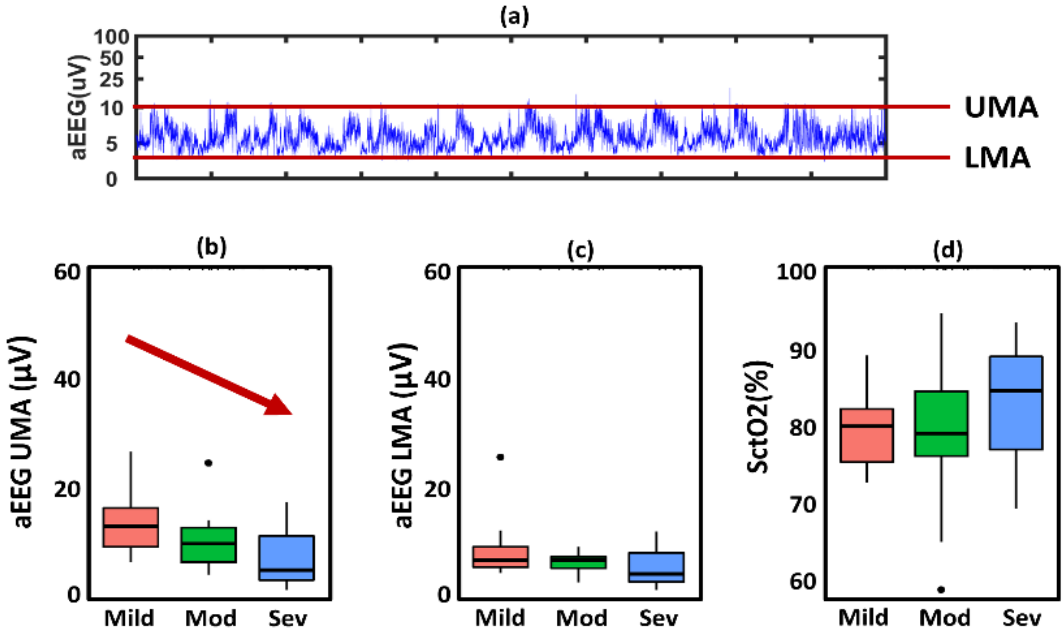

Figure 5-1. Boxplots showing mean upper and lower range of amplitude-EEG margins and percent tissue oxygen saturation among HIE neonates grouped in severity scale of encephalopathy.

5.3.2. NVC between Mild and Moderate encephalopathy

At group level, Fig. 5-2(a) describes the percentage of mean significant in-phase coherence over the entire wavelet scale range, plotted for 15 ‘mild’ (color coded in red) and 14 ‘moderate’ HIE neonates (color coded in blue). The shaded region in the background indicates the standard error of coherence, color coded for respective groups of neonates. The ‘mild’ group indicated a higher percent of coherence between SctO2 and aEEG than the ‘moderate’ group in the wavelet scale range of 16-64 minute (which is consistent with our previous finding), followed by a gradual descent over lower frequency range. Although the ‘moderate’ HIE group consistently showed higher coherence in the lower range of frequencies, however, according to this figure, the most distinct differences between infants with mild vs. moderate encephalopathy grade were observed in a very low-frequency (VLF) range of 0.00007–0.0001 Hz (wavelet scale s = 163–230 minute), shaded in green. The boxplot distribution Fig. 5-2(b) shows significant differences in NVC coherence between groups in the selected scale range. NVC coherence

was significantly lower in newborns with ‘mild’ encephalopathy compared to ‘moderate’ group (p = 0.005).

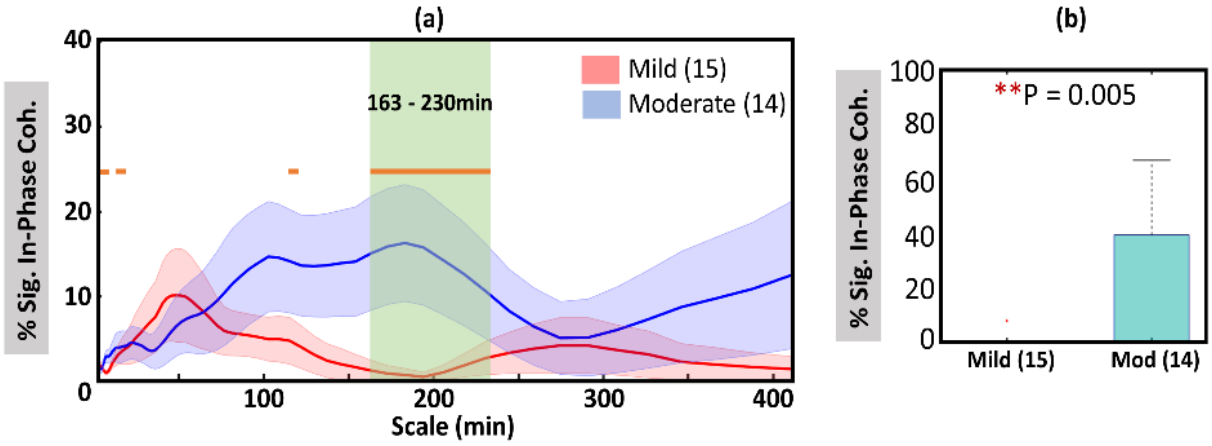

Figure 5-2. Significant SctO2→ aEEG in-phase coherence from newborns quantified in ‘mild’ (n=15) and ‘moderate’ (n=14) encephalopathy group

5.3.3. NVC between Mild, Mild_to_Moderate, and Moderate encephalopathy

At group level, Fig. 5-3(a) describes the percentage of mean significant in-phase coherence over the entire wavelet scale range, plotted for 15 ‘mild’ (color coded in red), 4 ‘Mild_to_Moderate (MM)’ (color coded in blue), and 14 ‘moderate’ HIE neonates (color coded in black). According to this figure, the most distinct differences between three groups of infants were observed in a very low-frequency (VLF) range of 0.0001–0.0002 Hz (wavelet scale *s* = 64–87 minute), shaded in green. The boxplot distribution Fig. 5-3(b, c) shows significant differences in NVC coherence between MM and other groups in the selected scale range, (p = 0.02 between MM and mild; p=0.03 between MM and moderate).

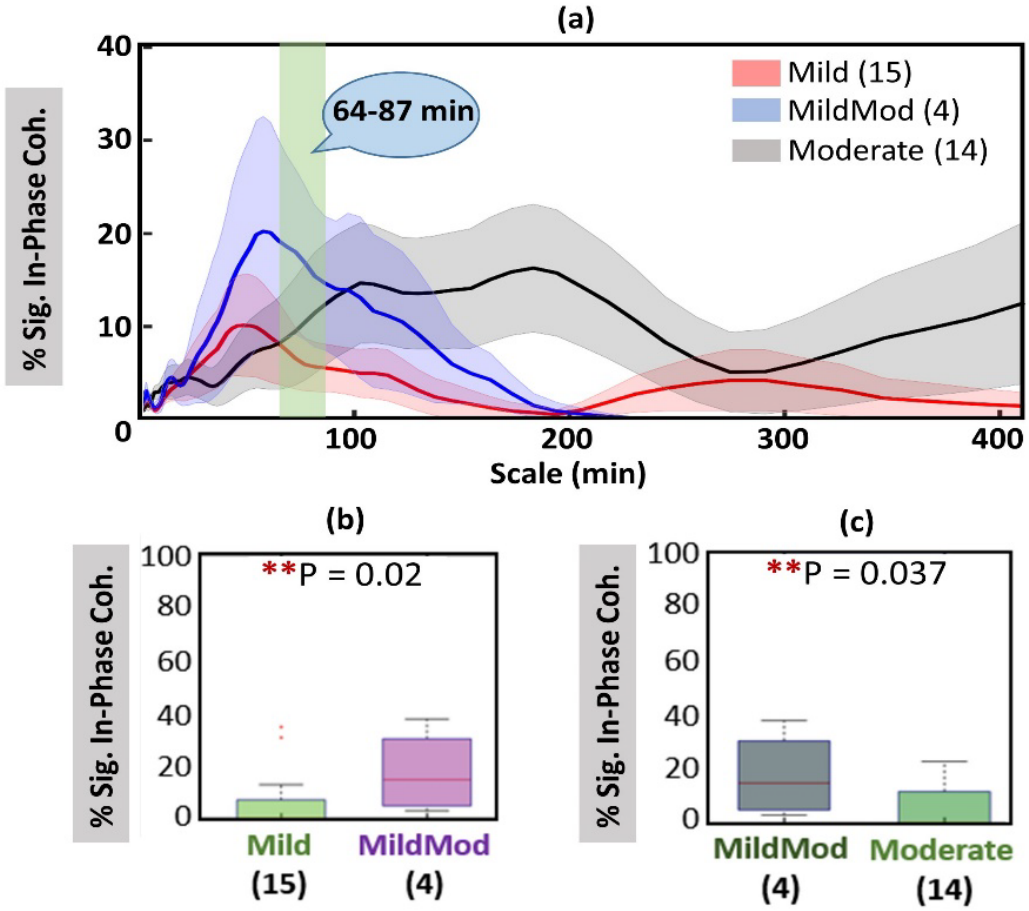

Figure 5-3. Significant SctO2→ aEEG in-phase coherence from newborns quantified in 'mild' (n=15), 'Mild_to_Moderate' (n=4) and 'moderate' (n=14) encephalopathy group. *** Need to add notes for (a), (b), and (c).

5.3.4. NVC between Mild, Moderate and Severe encephalopathy

At group level, Fig. 5-4 describes the percentage of mean significant in-phase coherence over the entire wavelet scale range, plotted for 15 'mild' (color coded in red), 14 'moderate' (color coded in blue), and 3 'severe' HIE neonates (color coded in black). The standard error deviation in the significant in-phase coherence numbers of 'severe' HIE group is notably large in a wavelet scale range of 150-300 minute. This is due to the possible influence of polynomial detrending effect of the wavelet in the very low frequency region of one of the three 'severe' HIE neonate. According to Fig. 5-4(left), the most distinct differences between three groups of infants were observed in a very low-frequency (VLF) range of

0.0001–0.0002 Hz (wavelet scale *s* = 75–125 minute), shaded in green. The boxplot distribution in Fig. 5-4(right) shows significant differences in NVC coherence between severe and other groups in the selected scale range, (p = 0.04 between severe and mild; p=0.04 between severe and moderate).

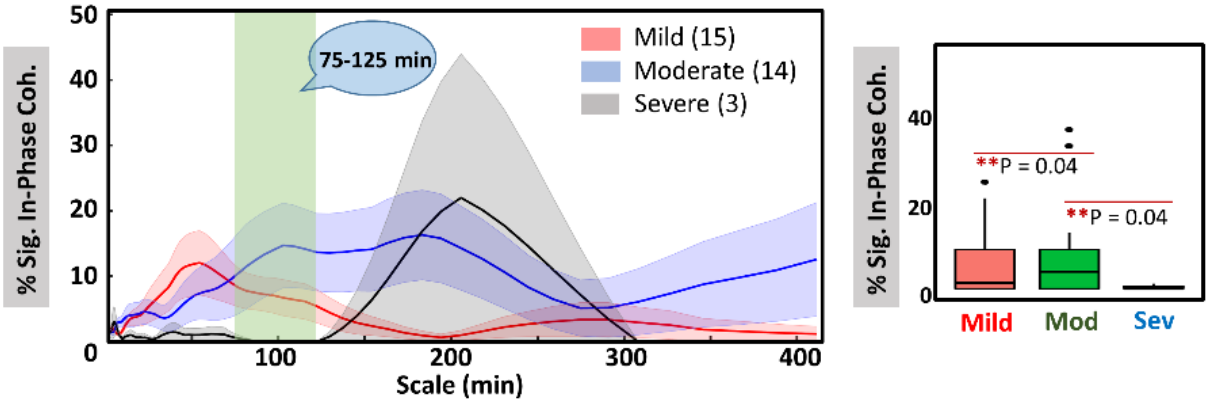

Figure 5-4. Significant SctO2→ aEEG in-phase coherence from newborns quantified in 'mild' (n=15), 'moderate' (n=14) and 'severe' (n=3) encephalopathy group. *** Need to add (a) and (b) and respective description

5.4. Discussion

Using scale-dependent percentage of wavelet-based significant in-phase coherence, it was possible to identify specific frequency regions where each encephalopathy group can be significantly differentiated from the rest in the first day of life. Although the 'mild' and 'moderate' HIE groups show statistically significant difference in the in low-frequency range of 0.00007–0.0001 Hz (wavelet scale *s* = 163–230 minute), the significant squared cross-wavelet coherence between SctO2 and aEEG detected by WTC in this frequency region inhibits high possibility to be influenced by polynomial detrending effect of the wavelet and as a result, the data cannot be trusted. The group of neonates who were initially classified into 'mild' encephalopathy group based on clinical sarnat examination within 6 hours of birth, and later escaladed to 'moderate' HIE category, show significant difference in percentage of in-phase coherence in the frequency range of 0.0001–0.0002 Hz (corresponding wavelet scale *s* = 64–87 minute), where they can be distinguished from both 'mild' and 'moderate' HIE groups. Although a specific wavelet scale

range (*s* = 75–125 minute) was identified to stratify encephalopathy spectrum of severe group, the low sample size of the 'severe' HIE group accounts for low reliability in the findings. Investigation of upper and lower range of amplitude aEEG margins among HIE neonates grouped in severity scale of encephalopathy demonstrates near-to-accurate prediction of sarnat scoring.

5.5. Conclusion

Using scale-dependent percentage of wavelet-based significant in-phase coherence, it was possible to identify specific frequency regions where each encephalopathy group can be significantly differentiated from the rest in the first day of life. Although the assessment of the scale-dependent percentage of wavelet-based significant in-phase coherence showed behavioral trends specific to each encephalopathy group, this cannot be used as a novel physiological biomarker yet to stratify the spectrum of encephalopathy severity in HIE neonates. Further investigation with a bigger sample size of each encephalopathy severity group is needed in future studies.

Chapter 6

Future Work

6.1. Exploring Dynamic Time Warping as a Non-Linear Approach to Investigate Brain Abnormalities in Neonatal Encephalopathy in the First Day of Life

6.1.1. Introduction

Neurovascular coupling (NVC) refers to the regulation mechanism that temporarily and regionally links the transient neural activity to the subsequent change in cerebral blood flow (CBF)[70-72]. NVC is measured using aEEG and SctO2 signals. Brain constitutes approximately 2% of our body weight but uses 20% of our body energy[73]. Most of its energy is used to fuel electrical impulses that neurons employ to generate action potentials by continuous exchange of charged ions in and out of the cell, a phenomenon commonly known as depolarization and repolarization. Lack of sufficient energy reserves is responsible for high dependency of our brain on constant/controlled delivery of substrate (oxygen and glucose) and removal of by-products of metabolism for uninterrupted flow of various biological processes[74], which are transported to/from the brain by different arterial systems (pial arteries[75] and penetrating arterioles[76]). Any alteration in cellular interactions between neurons, glia and cerebral blood vessels (known as neurovascular unit) leads to vasodilation and vasoconstriction, and thereby impairs the ability of the brain to provide sufficient flow to the active regions, resulting in brain dysfunction[77].

There has been a growing interest in studying relationship between the brain's electrical activity and hemodynamic activity. In the adult brain, CBF is distributed according to the functional activity of the brain with evidence of increase in blood flow mainly at the part of the brain responsible for higher activity (verbal, motor, visual), a mechanism commonly termed as functional hyperaemia[77,78]. This change in measured response has been proven to be a good surrogate measurement for NVC and has been exploited by many investigators to map adult brain functions using spatiotemporal studies that link

changes in local blood flow to an artificially applied stimulus[79,80]. Observations from some of the studies on the adult normal brain have reported localized changes in blood flow following neural activation, such as increase in pulsation in the frontal lobe after performing arithmetic calculation and increase blood flow to the occipital lobe following its activation, providing evidence to this controlled delivery of substrates[78,81]. But most of these studies have been conducted in adult population and currently there are only a handful of studies exploring whether these mechanisms work the same way in neonates compared to adults[77,82].

In general, the dynamics of linear and non-linear brain signal interactions should be taken into account before quantification of NVC. In signal processing terms, signal interactions are regarded as the degree to which signals arising from different cortical sources resemble one another. In neonates, some of the most commonly used methods to describe linear correlation between two signals with different lags or frequencies are cross-correlation function (CCF), magnitude squared coherence (MSC), and wavelet transform coherence (WTC). A coupling between electroencephalogram (EEG) and near-infrared spectroscopy (NIRS) in premature neonates using MSC have indicated augmented signal interaction in neonates without brain injury[83]. Dynamic oscillations and correlations between EEG and NIRS were measured using WTC in HIE neonates[4]. Caicedo et al. quantified directionality between NIRS and EEG using a linear metric transfer entropy (TE)[84]. A recent study by Hendrikx et al. computed the coupling between the brain electrical activity and oxygenation in premature neonates using linear and non-linear approaches[85]. But to the best of our knowledge, not many studies have utilized non-linear signal processing techniques to compute NVC in neonates.

In this chapter, we will explore dynamic time warping (DTW) as a non-linear measure to monitor coupling between the EEG and SctO2 of HIE neonates in the first day of life based on some preliminary results. The rational for using or finding another method, such as a non-linear approach, to quantify NVC is justified by the fact that WTC requires the completion of continuous recordings in long hours (e.g., >20 hours) in order to obtain accurate and meaningful results. There is no output or outcome from WTC analysis during or in the middle of hours-long recording. On the other hand, DTW-derived metrics can

provide hourly results, overcoming the weakness of WTC. In the following, I assessed the predictive ability of such non-linear approach and examined whether DTW could identify neonates with brain injury in the first day of life.

6.1.2. Materials and methods

The study population and measurement protocol were already reported in Sections 4.2.1. The Neuroimaging assessments and monitoring steps with EEG and NIRS were also described in Sections 4.2.3. and 4.2.4., respectively.

6.1.2.1. Dynamic time warping (DTW)

DTW is a non-linear time series alignment technique that measures the similarity between two locally out of phase, time-dependent series in temporal domain. It determines the optimal alignment between two sequences by converting the time series data into vectors and calculating the Euclidean distance between those points in vector space. In order to align two time series signals, A =$\{X_1, X_2 \dots, X_N\}$and B = $\{Y_1, Y_2 \dots, Y_N\}$, where 'N' represents the length of simultaneously recorded A and B. Euclidean distance between each element of the two sequences is calculated to provide a distance matrix (Da) of size $N \times N$, which is used to determine the best possible alignment between the two signals. Each element of this matrix is the shortest distance from the origin to that element. The shortest accumulated distance for an element at position (i, j) in matrix Da is calculated by the formula,

$$Da = |\mathrm{A}(i) - \mathrm{B}(j)| + \min [Da(i, j\text{-}1), Da(i\text{-}1, j), Da(i\text{-}1, j\text{-}1)],$$

where A (i) and B (j) are the amplitude values of the time series A and B at i^{th} and j^{th} location, respectively, and $Da(i, j\text{-}1)$, $Da(i\text{-}1, j)$, $Da(i\text{-}1, j\text{-}1)$ are the accumulated distance of the previous neighboring nodes[86]. Once the entire distance matrix is computed, the shortest distance between Da (N, N) and Da (1, 1) is calculated. Starting from location Da ($i = \mathrm{N}, j = \mathrm{N}$), the warping path is constructed through the distance matrix by taking the minimum distance of three previous neighboring nodes Da (i, j-

1), $Da\ (i\text{-}1, j)$, $Da\ (i\text{-}1, j\text{-}1)$ from its current location, until it reaches $Da\ (1, 1)$[86,87]. This warping path describes the best alignment between two time series.

6.1.2.2. Quantification of DTW derived metrics

We used a MATLAB-based software package to perform non-linear time alignment using DTW between the oscillations of NIRS-SctO2 and aEEG, recorded simultaneously for 20 hours in the first day of life. Both the signals are time-aligned and segmented into twenty equal non-overlapping windows of duration 1 hour each, for each window optimal warping path between length of SctO2 and aEEG was calculated. The warped path between signals (represented in blue) along with straight line fit between them (represented in red) are plotted with SctO2 along the x-axis and aEEG on the y-axis in Figure 6-1. The deviation of warping path from the straight-line fit represent lead by aEEG (above the warping path) and SctO2 (below the warping path) signals, respectively, at various instants of time. The deviation of warping path in each window is restricted within 100 samples (approx. distance of 8 minute, 100/0.209/60 = 7.97 ~ 8 minute) in either direction from a straight-line fit between input signals, limiting the maximum possible area of deviation (MAD) in case of 100% non-uniformity between the signals, i.e. MAD = 100 × window length. The deviation from warped path and straight-line fit is represented as relative area under the curve (AUC) for positive and negative deviation (above and below the diagonal). Given the fact that only one signal can lead at one time, relative AUC for percent-MADMAD that aEEG precedes SctO2 in each hour is estimated as the ratio of aggregated positive AUC to MAD. Similarly, relative AUC for percent MAD that SctO2 signal precede aEEG in each hour is estimated as ratio of aggregated negative AUC to MAD. The relative AUC of lead by aEEG and SctO2 across each hour is calculated for neonates of normal and abnormal injury groups and used as a biomarker to stratify the spectrum of encephalopathy severity between them.

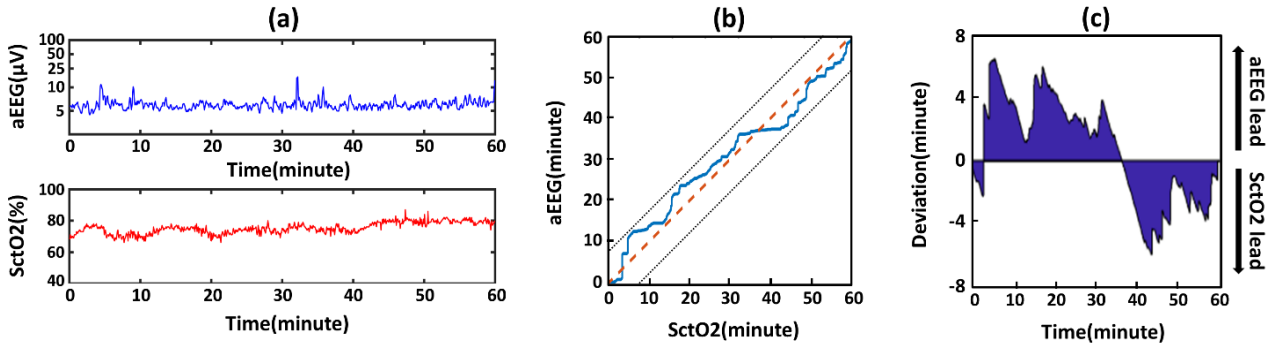

Figure 6-1. Implementation of dynamic time warping (DTW). (a) Example of a 1-hour aEEG and SctO2 signal recorded with a0.209-Hz sampling frequency. (b) It shows best time aligned path (shown in blue) between the spontaneous oscillations of aEEG (plotted along y-axis) and SctO2 (plotted along x-axis). (c) It shows positive and negative deviation of the warping path from the diagonal, represented as shaded AUC in violet.

As an example, Fig. 6-1(a) shows traces of 1-hour aEEG and SctO2 signal, sampled at 0.209-Hz from a neonate with normal MRI outcome. The y-axis of aEEG represents amplitude in microvolt and is plotted in linear logarithmic scale and y-axis of SctO2 signal is represented in percent of SctO2. The x-axis of both the traces represents time in minute. Fig. 6-1(b) shows the DTW path between the spontaneous oscillations of aEEG (plotted along y-axis) and SctO2 (plotted along x-axis) from Fig. 6-1(a). The optimal warping path (represented in blue) describes the best time alignment between the two signals, and red dotted line through the diagonal represents the straight-line fit between them. The warping path is restricted to 100 samples (approx. 8 minute) on either side of the diagonal and is marked as black dotted lines. The deviation of the warping path above and below the diagonal is represented as shaded AUC in violet in Fig. 6-1(c), which describes the relative AUC for percent-MAD lead by aEEG and SctO2 signal, respectively, at various instants during 1-h recording.

6.1.3. Results

6.1.3.1. Assessment of DTW-derived metrics on entire cohort

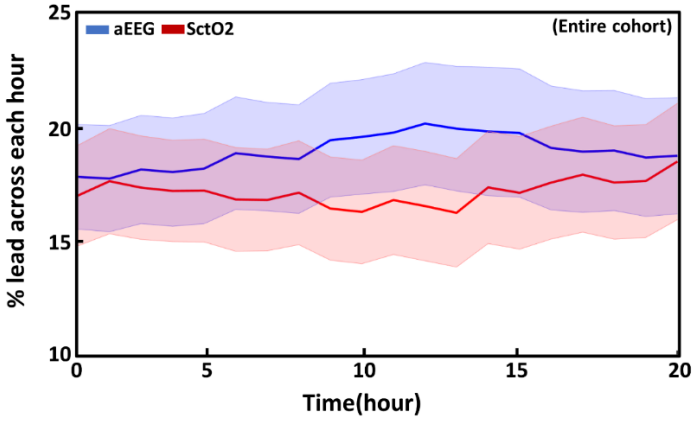

Figure 6-2. Relative AUC for percent-MAD lead by aEEG (represented in blue) and SctO2 (represented in red) signals across each hour in entire cohort of HIE neonates, irrespective of their MRI outcome

In Fig. 6-2, the mean curves of relative AUC for percent-MAD lead by aEEG (represented in blue) and SctO2 (represented in red) across each hour of 20-h recording are plotted for the entire cohort of HIE neonates. The blue and red shaded area at the background represents standard error for percent-MAD lead by aEEG and SctO2, respectively across neonates. The figure provides a visualization and highlights the fact that aEEG tends to lead for a higher percent of MAD compared to SctO2 across each hour in the first day of life. However, there is no evidence of statistical difference between the percent lead by both the signals observed across any hour.

6.1.3.2. Assessment of DTW-derived metrics between normal and abnormal MRI groups

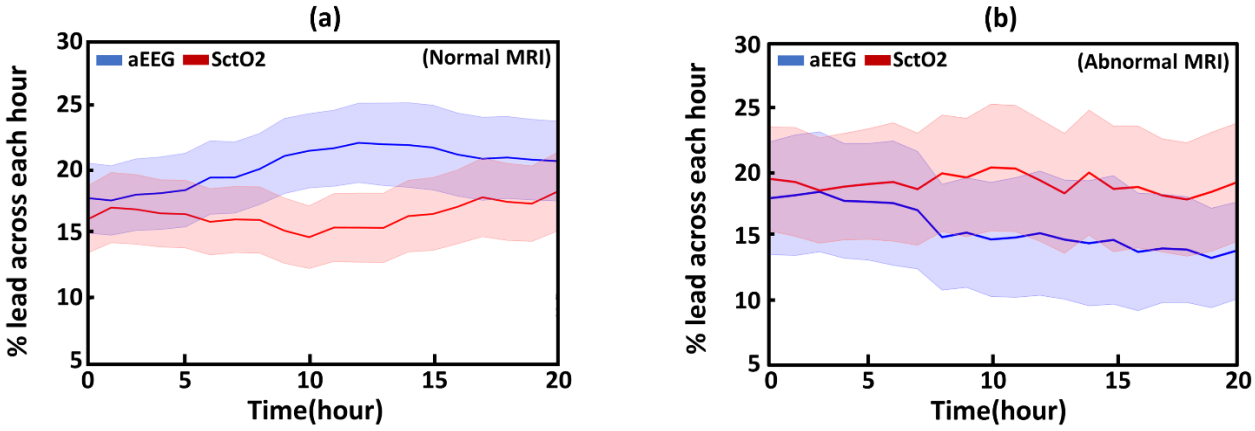

Figure 6-3. Comparison between normal and abnormal MRI groups: Fig. 6-3a and Fig. 6-3b represent curves for normal and abnormal MRI group, respectively. In each of these figures, blue and red solid lines represent the relative AUC for percent-MAD lead by aEEG and SctO2 signals, respectively, across each hour.

Fig. 6-3 shows a comparison between the groups with normal and abnormal MRI based on the relative AUC for percent-MAD lead by aEEG and SctO2 across hours. The blue and red solid lines represent the mean curves of percent-MAD lead by aEEG and SctO2 for both the groups. In group level, aEEG tends to lead SctO2 for a higher percent of MAD in the normal group in day 1 since birth, whereas an opposite trend (i.e. SctO2 leads aEEG for high percent of MAD) is evident in the abnormal group.

6.3.3. Statistical analysis

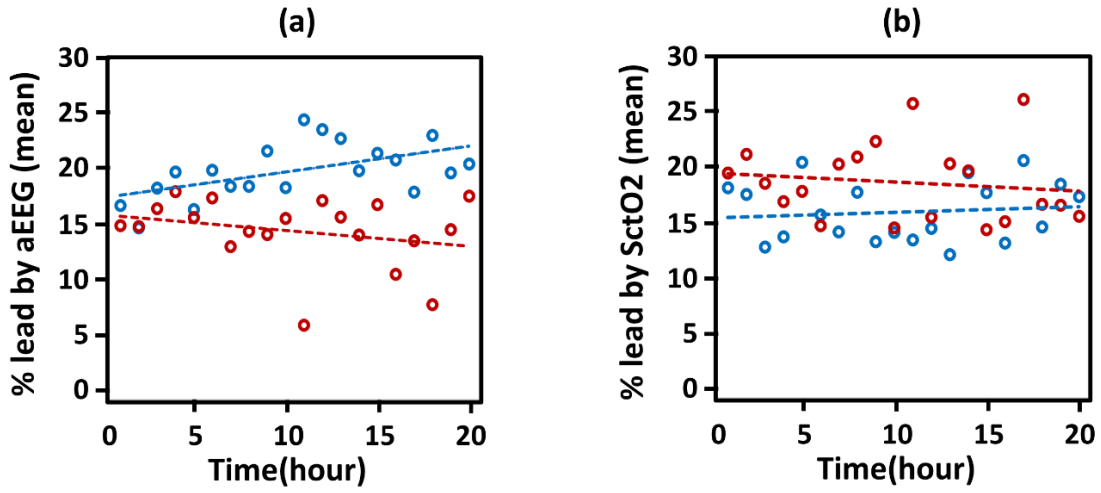

Figure 6-4: Statistical analysis between normal (blue) and abnormal (red) MRI groups based on (a) relative AUC in percent MAD led by aEEG and (b) relative AUC led by SctO2 using linear regression fittings. Significant difference ($p = 0.04$) between normal and abnormal groups was observed in percent MAD by aEEG signal across time since birth.

Fig. 6-4a shows the linear regression fittings for the relative AUC in percent MAD led by aEEG in the normal (represented in blue) and abnormal MRI groups (represented in red) using mean summary

statistics. In group level, an increase in the slope of percent aEEG lead across hours from birth is observed in neonates with no abnormalities, whereas a decrease in slope is observed in neonates with abnormalities. Fig. 6-4b shows the linear regression models for the relative percent of time lead by SctO2 between the two groups using mean summary statistics. No major difference in the slope of percent SctO2 lead across time since birth is observed in the first day of life between two groups (Fig. 6-4b).

There was a significant difference in % aEEG lead trajectories (Fig. 6-4a), with greater decline in % aEEG for neonates in the abnormal MRI group compared with the normal group (-0.462; $p = 0.024$). However, there was no significant difference in % SctO2 lead slopes (Fig. 6-4b) for neonatal patients in the abnormal vs normal MRI groups (-0.132; $p = 0.512$).

6.1.4. Discussion

The current study assessed a non-linear relationship between the dynamic oscillations of aEEG and SctO2 recorded in the HIE neonates using a dynamic time warping technique. The relative AUCs in percent-MAD led by aEEG and SctO2 signals, respectively, across each hour in the first day of life were evaluated and compared between the normal and abnormal groups to study if the change of AUC in percent-MAD over time is an indication of developing abnormality in neonates. The preliminary results of the relative AUC in percent-MAD led by aEEG signal, calculated every hour in normal MRI group, show gradual increase over time in the first day of life, whereas a negative trend or decrease in the relative AUC in percent-MAD led by aEEG signal is observed in neonates with abnormal MRI.

Brain MRI performed within a week of birth is a proxy indicator of neurodevelopmental outcome at 18-24 months of age[58]. Several studies conducted on neonates have suggested strong correlation between aEEG recorded within 72 HOL and cranial MRI assessments at term equivalent age[88-90]. On contrary, SctO2 signal has shown little to no association with indication of abnormalities[37,91]. These reports are evidence to support our preliminary findings that aEEG recorded in the first day of life had gradual and significant changes of relative AUC in percent-MAD across hours between normal and

abnormal MRI groups, while SctO2 concurrently recorded had no significant changes in percent-MAD between the two groups.

However, a major drawback of DTW is the scale (i.e., width of the alignment path) dependent nature of the algorithm. Since the algorithm measures the Euclidean distance between two signals only within a predefined perimeter, increase in the perimeter/boundary of search allows comparison between more neighboring locations with possibility of better time alignment. As a result, warping paths between the signals vary significantly with the change in search radar. To justify this statement, I selected two 1-h segments of aEEG and SctO2 signal and calculated relative AUC values led by two respective signals each time with variable search radars of (a) 8 minute, (b) 4 minute, and (c) 2 minute, respectively.

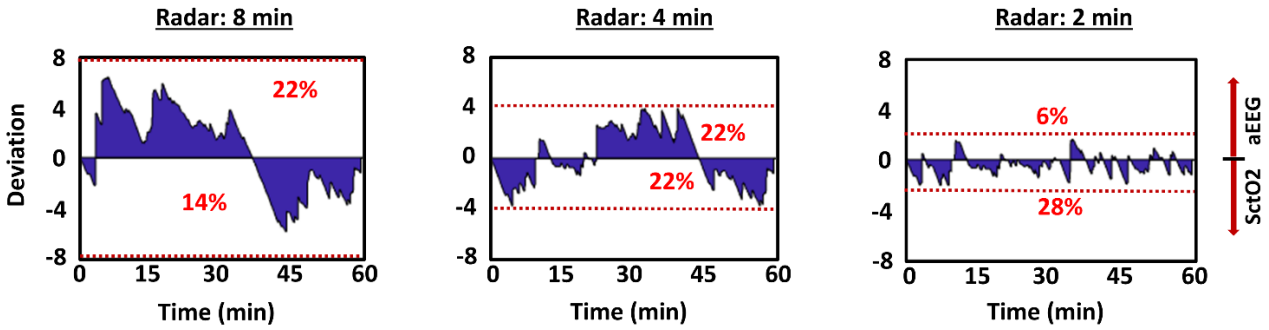

Figure 6-5: Scale dependency of DTW

Fig. 6-5 demonstrates the scale dependency nature of DTW algorithm. Y-axis represents deviation of aEEG and SctO2 signals from the perfect time alignment between them, and x-axis represents length of signals in minute. Figures on the left, middle and right show relative AUC estimation in percent-MAD led by aEEG (>0) and by SctO2 (<0) when the search for similarity is restricted to 8 minute, 4 minute, and 2 minute, respectively. As evident from the figure, AUC estimations in relative percent-MAD led by signals are inconsistent among the three cases and highly dependent on the length of search radar. Since there is no concrete evidence of aEEG and SctO2 signals always leading one another within a certain time margin in neonates, based on a random selection of similarity search perimeter (8 minute, or, 100 samples in this study) we are unable to conclude if DTW is an appropriate method to

investigate changes in brain hemodynamics in HIE neonates. This calls for better non-linear metric to study NVC that is independent of scale.

Hendrikx et. al in their assessment of TE in preterm neonates indicated the possibility of two different mechanisms affecting NVC simultaneously.[85] While linear measures such as cross-correlation function, magnitude squared coherence and wavelet transform coherence can determine coupling between aEEG and NIRS, these methods cannot detect the non-linear mechanisms affecting NVC. The preliminary findings from my study points out that evolving encephalopathy alters the percent-MAD led by aEEG in neonates in their first day of life, and that this alteration can be captured using non-linear DTW approach. However, percent-MAD lead of signals estimated by DTW-derived relative AUC metric shown in this study cannot be used as of now to predict signal trends associated with brain abnormality due to inconsistency in results with variation in search radars. Other DTW-derived metrics, such as Euclidean distance and amount of time deviation from the perfect alignment every hour, need to be further explored in the future for finding their consistency with respect to variation in scale and predictive ability in early identification of brain abnormality in neonates with HIE.

6.2. Other scopes

- Although NVC proved to accurately predict the neonates with abnormalities in the first day of life, the prediction was based on MRI results as a proxy indicator of neurodevelopmental outcome at 18-24 months. On completion of the follow-up assessment of brain status of the entire cohort at 18-24 months, the findings by NVC need to be validated and further tested on a larger cohort.
- The asphyxiated neonates (with moderate and severe HIE) in the current study at Parkland hospital in Dallas were randomly assigned in one of the two trial studies, study 1- where the neonate was given EPO (every 24-h) with hypothermia, study 2- the neonate got conventional hypothermia treatment. EPO is associated with acute improvement of NVC. The focus of future

work will be to compare the effects of EPO + hypothermia vs. hypothermia alone on the real time NVC measures in the moderate-to-severe NE group who are currently offered therapies.

- EEG is currently being monitored across 8 locations on the neonatal scalp. However, the studies shown in this dissertation considered electrical activity from only the central region (C3-C4) to perform NVC with NIRS-SctO2. Several studies have also reported effects of encephalopathy in parietal and occipital regions in those neonates. Comparison between NVC measures from the central region and other brain regions is a potential future direction of work.
- Study of information flow between different brain regions of HIE neonates using functional connectivity methods may provide a good understanding of the global brain injury. Also, further studies can be explored to investigate the brain's electrophysiological activation and oxygenation during various phases of treatments that include hypothermia and normothermia to identify neonates who may need additional intervention.

Chapter 7

Conclusion

In conclusion, the dissertation has accomplished the following objectives towards prediction of brain injury in neonates with hypoxic ischemic encephalopathy:

1. Demonstrated that WTC-based NVC is not impacted by variation in aEEG outputs driven by different algorithms, which thereby suggests that NVC is a robust and reliable methodology for quantifying NVC.
2. Confirmed that raw EEG with a one-step resampling can be used to perform NVC assessment with NIRS-SctO2 instead of hovering through several unspecific data processing pipelines to obtain aEEG. The study however indicates that, this finding reduces complexities more in the post processing steps in signal-processing domain that can potentially enhance the translational rigor of real-time physiological biomarkers in future. But for the immediate convenience of clinicians by the bedside, use of aEEG is still recommended over raw EEG.
3. Demonstrated the feasibility of using dynamic wavelet transform coherence analysis to assess neurovascular coupling (NVC) by the bedside in the first day of life. Preliminary results suggest that quantification of NVC performed within the first day of life can successfully predict possibilities or probabilities of MRI-shown injuries that may develop in a few days later in the newborns despite of their initial grade of encephalopathy to be either mild or moderate.
4. Using scale-dependent percentage of wavelet-based significant in-phase coherence, it was possible to identify specific frequency regions where each encephalopathy group can be significantly differentiated from the rest in the first day of life. However, this approach is not proven as a novel physiological biomarker yet to stratify the spectrum of encephalopathy severity in HIE neonates due to evolving nature of encephalopathy. Further investigation with a bigger sample size of each encephalopathy severity group is recommended.

References

1 Hellstrom-Westas, L., Rosen, I. & Svenningsen, N. W. Predictive value of early continuous amplitude integrated EEG recordings on outcome after severe birth asphyxia in full term infants. *Arch Dis Child Fetal Neonatal Ed* **72**, F34-38, doi:10.1136/fn.72.1.f34 (1995).

2 de Vries, L. S. & Hellstrom-Westas, L. Role of cerebral function monitoring in the newborn. *Arch Dis Child Fetal Neonatal Ed* **90**, F201-207, doi:90/3/F201 [pii] 10.1136/adc.2004.062745 (2005).

3 Zhang, D. & Ding, H. Calculation of compact amplitude-integrated EEG tracing and upper and lower margins using raw EEG data. *Health* **Vol. 5**, 885-891 (2013).

4 Chalak, L. F. *et al.* Novel Wavelet Real Time Analysis of Neurovascular Coupling in Neonatal Encephalopathy. *Sci Rep* **7**, 45958, doi:10.1038/srep45958 (2017).

5 Werther, T. *et al.* Are All Amplitude-Integrated Electroencephalogram Systems Equal? *Neonatology* **112**, 394-401, doi:10.1159/000480008 (2017).

6 Vesoulis, Z. A. *et al.* WU-NEAT: A clinically validated, open- source MATLAB toolbox for limited-channel neonatal EEG analysis. *arXiv* **1805.04566v1** (2018).

7 McClellan, J. H. & Parks, T. W. A personal his- tory of the Parks-McClellan algorithm. *IEEE Signal Process Magazine* **22**, 82-86 (2005).

8 Grinsted, A., Moore, J. C. & Jevrejeva, S. Application of the cross wavelet transform and wavelet coherence to geophysical time series. (2004).

9 Greisen, G. Is near-infrared spectroscopy living up to its promises? *Semin Fetal Neonatal Med* **11**, 498-502, doi:S1744-165X(06)00077-1 [pii] 10.1016/j.siny.2006.07.010 (2006).

10 Toet, M. C., Lemmers, P. M., van Schelven, L. J. & van Bel, F. Cerebral oxygenation and electrical activity after birth asphyxia: their relation to outcome. *Pediatrics* **117**, 333-339 (2006).

11 Ancora, G. *et al.* Early predictors of short term neurodevelopmental outcome in asphyxiated cooled infants. A combined brain amplitude integrated electroencephalography and near infrared spectroscopy study. *Brain and Development* **35**, 26-31 (2013).

12 Levene, M. L., Kornberg, J. & Williams, T. The incidence and severity of post-asphyxial encephalopathy in full-term infants. *Early human development* **11**, 21-26 (1985).

13 Hellstrom-Westas, L. Continuous electroencephalography monitoring of the preterm infant. *Clin Perinatol* **33**, 633-647, vi, doi:10.1016/j.clp.2006.06.003 (2006).

14 De Vries, L. & Hellström-Westas, L. Role of cerebral function monitoring in the newborn. *Archives of Disease in Childhood-Fetal and Neonatal Edition* **90**, F201-FF207 (2005).

15 Das, Y. *et al.* Rigor of Neurovascular Coupling (NVC) Assessment in Newborns Using Different Amplitude EEG Algorithms. *Scientific Reports* **10**, 1-9 (2020).

16 Maynard, D., Prior, P. F. & Scott, D. F. Device for continuous monitoring of cerebral activity in resuscitated patients. *Br Med J* **4**, 545-546, doi:10.1136/bmj.4.5682.545-a (1969).

17 Zhang, D. & Ding, H. Calculation of compact amplitude-integrated EEG tracing and upper and lower margins using raw EEG data. (2013).

18 Vesoulis, Z. A. *et al.* WU-NEAT: A clinically validated, open-source MATLAB toolbox for limited-channel neonatal EEG analysis. *arXiv preprint arXiv:1805.04566* (2018).

19 Dyer, S. A. & Dyer, J. S. Cubic-spline interpolation. 1. *IEEE Instrumentation & Measurement Magazine* **4**, 44-46 (2001).

20 Tian, F. *et al.* Regional heterogeneity of cerebral hemodynamics in mild neonatal encephalopathy measured with multichannel near-infrared spectroscopy. *Pediatric Research*, 1-9 (2020).

21 Shalak, L. F., Laptook, A. R., Velaphi, S. C. & Perlman, J. M. Amplitude-integrated electroencephalography coupled with an early neurologic examination enhances prediction of term infants at risk for persistent encephalopathy. *Pediatrics* **111**, 351-357 (2003).

22 Gluckman, P. D. *et al.* Selective head cooling with mild systemic hypothermia after neonatal encephalopathy: multicentre randomised trial. *The Lancet* **365**, 663-670 (2005).
23 Shah, N. A. & Wusthoff, C. J. How to use: amplitude-integrated EEG (aEEG). *Archives of Disease in Childhood-Education and Practice* **100**, 75-81 (2015).
24 Olischar, M. *et al.* Reference values for amplitude-integrated electroencephalographic activity in preterm infants younger than 30 weeks' gestational age. *Pediatrics* **113**, e61-66, doi:10.1542/peds.113.1.e61 (2004).
25 Vesoulis, Z. A. *et al.* Normative amplitude-integrated EEG measures in preterm infants. *Journal of Perinatology* **35**, 428-433 (2015).
26 Thornberg, E., Thiringer, K., Odeback, A. & Milsom, I. Birth asphyxia: incidence, clinical course and outcome in a Swedish population. *Acta paediatrica* **84**, 927-932 (1995).
27 Volpe, J. J. Neonatal encephalopathy: an inadequate term for hypoxic–ischemic encephalopathy. *Annals of neurology* **72**, 156-166 (2012).
28 Jacobs, S. E. *et al.* Cooling for newborns with hypoxic ischaemic encephalopathy. *Cochrane database of systematic reviews* (2013).
29 Azzopardi, D. *et al.* Effects of hypothermia for perinatal asphyxia on childhood outcomes. *New England Journal of Medicine* **371**, 140-149 (2014).
30 Karnatovskaia, L. V., Wartenberg, K. E. & Freeman, W. D. Therapeutic hypothermia for neuroprotection: history, mechanisms, risks, and clinical applications. *The Neurohospitalist* **4**, 153-163 (2014).
31 Toet, M. C., van der Meij, W., de Vries, L. S., Uiterwaal, C. S. & van Huffelen, K. C. Comparison between simultaneously recorded amplitude integrated electroencephalogram (cerebral function monitor) and standard electroencephalogram in neonates. *Pediatrics* **109**, 772-779 (2002).
32 Meek, J. H. *et al.* Abnormal cerebral haemodynamics in perinatally asphyxiated neonates related to outcome. *Archives of Disease in Childhood-Fetal and Neonatal Edition* **81**, F110-F115 (1999).
33 van Bel, F. *et al.* Changes in cerebral hemodynamics and oxygenation in the first 24 hours after birth asphyxia. *Pediatrics* **92**, 365-372 (1993).
34 Ouwehand, S. *et al.* Predictors of Outcomes in Hypoxic-Ischemic Encephalopathy following Hypothermia: A Meta-Analysis. *Neonatology*, 1-17 (2020).
35 Thoresen, M., Hellström-Westas, L., Liu, X. & de Vries, L. S. Effect of hypothermia on amplitude-integrated electroencephalogram in infants with asphyxia. *Pediatrics* **126**, e131-e139 (2010).
36 Sabir, H. & Cowan, F. M. in *Seminars in Fetal and Neonatal Medicine.* 115-121 (Elsevier).
37 Shellhaas, R. A., Kushwaha, J. S., Plegue, M. A., Selewski, D. T. & Barks, J. D. An evaluation of cerebral and systemic predictors of 18-month outcomes for neonates with hypoxic ischemic encephalopathy. *Journal of child neurology* **30**, 1526-1531 (2015).
38 Peng, S. *et al.* Does near-infrared spectroscopy identify asphyxiated newborns at risk of developing brain injury during hypothermia treatment? *American journal of perinatology* **32**, 555-564 (2015).
39 Shellhaas, R. A. *et al.* Limited short-term prognostic utility of cerebral NIRS during neonatal therapeutic hypothermia. *Neurology* **81**, 249-255 (2013).
40 Drury, P. P., Gunn, E. R., Bennet, L. & Gunn, A. J. Mechanisms of hypothermic neuroprotection. *Clinics in perinatology* **41**, 161-175 (2014).
41 Gunn, A. J., Gunn, T. R., Gunning, M. I., Williams, C. E. & Gluckman, P. D. Neuroprotection with prolonged head cooling started before postischemic seizures in fetal sheep. *Pediatrics* **102**, 1098-1106 (1998).
42 Shankaran, S. *et al.* Whole-body hypothermia for neonates with hypoxic-ischemic encephalopathy. *N Engl J Med* **353**, 1574-1584, doi:10.1056/NEJMcps050929 (2005).

43 Zhou, W.-h. *et al.* Selective head cooling with mild systemic hypothermia after neonatal hypoxic-ischemic encephalopathy: a multicenter randomized controlled trial in China. *The Journal of pediatrics* **157**, 367-372. e363 (2010).
44 Jacobs, S. E. *et al.* Whole-body hypothermia for term and near-term newborns with hypoxic-ischemic encephalopathy: a randomized controlled trial. *Archives of pediatrics & adolescent medicine* **165**, 692-700 (2011).
45 Robertson, C. M. & Finer, N. N. Long-term follow-up of term neonates with perinatal asphyxia. *Clinics in perinatology* **20**, 483-499 (1993).
46 Sarnat, H. B. & Sarnat, M. S. Neonatal encephalopathy following fetal distress: a clinical and electroencephalographic study. *Archives of neurology* **33**, 696-705 (1976).
47 Lipper, E. G., Voorhies, T. M., Ross, G., Vannucci, R. C. & Auld, P. A. Early predictors of one-year outcome for infants asphyxiated at birth. *Developmental Medicine & Child Neurology* **28**, 303-309 (1986).
48 Chalak, L. F. *et al.* Neurodevelopmental outcomes after hypothermia therapy in the era of Bayley-III. *Journal of Perinatology* **34**, 629-633 %@ 1476-5543 (2014).
49 Rollins, N. *et al.* Predictive value of neonatal MRI showing no or minor degrees of brain injury after hypothermia. *Pediatric neurology* **50**, 447-451 %@ 0887-8994 (2014).
50 Tian, F., Tarumi, T., Liu, H., Zhang, R. & Chalak, L. Wavelet coherence analysis of dynamic cerebral autoregulation in neonatal hypoxic–ischemic encephalopathy. *NeuroImage: Clinical* **11**, 124-132 (2016).
51 Maraun, D. & Kurths, J. Cross wavelet analysis: significance testing and pitfalls. (2004).
52 Walsh, B. H. *et al.* The frequency and severity of magnetic resonance imaging abnormalities in infants with mild neonatal encephalopathy. *The Journal of pediatrics* **187**, 26-33. e21 (2017).
53 Chalak, L. F., Adams-Huet, B. & Sant'Anna, G. A total Sarnat score in mild hypoxic-ischemic encephalopathy can detect infants at higher risk of disability. *The Journal of pediatrics* **214**, 217-221. e211 (2019).
54 Chalak, L. & Legave, J.-M. Oryzalin combined with adventitious regeneration for an efficient chromosome doubling of trihaploid kiwifruit. *Plant Cell Reports* **16**, 97-100 (1996).
55 Chalak, L., Latremouille, S., Mir, I., Sánchez, P. J. & Sant'Anna, G. A review of the conundrum of mild hypoxic-ischemic encephalopathy: Current challenges and moving forward. *Early Human Development* **120**, 88-94 (2018).
56 Chalak, L. F. Best practice guidelines on management of mild neonatal encephalopathy: Is it really mild? *Early human development* **120**, 74 (2018).
57 Marlow, N. Is survival and neurodevelopmental impairment at 2 years of age the gold standard outcome for neonatal studies? *Archives of Disease in Childhood-Fetal and Neonatal Edition* **100**, F82-F84 (2015).
58 Shankaran, S. *et al.* Neonatal magnetic resonance imaging pattern of brain injury as a biomarker of childhood outcomes following a trial of hypothermia for neonatal hypoxic-ischemic encephalopathy. *The Journal of pediatrics* **167**, 987-993. e983 (2015).
59 Chalak, L. F. *et al.* Prospective research in infants with mild encephalopathy identified in the first six hours of life: neurodevelopmental outcomes at 18–22 months. *Pediatric research* **84**, 861-868 (2018).
60 Barkovich, A. J. *et al.* Prediction of neuromotor outcome in perinatal asphyxia: evaluation of MR scoring systems. *American Journal of Neuroradiology* **19**, 143-149 (1998).
61 Haataja, L. *et al.* Neurologic examination in infants with hypoxic-ischemic encephalopathy at age 9 to 14 months: use of optimality scores and correlation with magnetic resonance imaging findings. *The Journal of pediatrics* **138**, 332-337 (2001).
62 Sie, L. T. L. *et al.* MR patterns of hypoxic-ischemic brain damage after prenatal, perinatal or postnatal asphyxia. *Neuropediatrics* **31**, 128-136 %@ 0174-0304X (2000).
63 Miller, S. P. *et al.* Patterns of brain injury in term neonatal encephalopathy. *The Journal of pediatrics* **146**, 453-460 %@ 0022-3476 (2005).

64 Belet, N. *et al.* Hypoxic-ischemic encephalopathy: correlation of serial MRI and outcome. *Pediatric neurology* **31**, 267-274 %@ 0887-8994 (2004).
65 Steinman, K. J. *et al.* Neonatal watershed brain injury on magnetic resonance imaging correlates with verbal IQ at 4 years. *Pediatrics* **123**, 1025-1030 %@ 0031-4005 (2009).
66 van Kooij, B. J. M. *et al.* Serial MRI and neurodevelopmental outcome in 9-to 10-year-old children with neonatal encephalopathy. *The Journal of pediatrics* **157**, 221-227. e222 %@ 0022-3476 (2010).
67 Laptook, A. R. *et al.* Effect of therapeutic hypothermia initiated after 6 hours of age on death or disability among newborns with hypoxic-ischemic encephalopathy: a randomized clinical trial. *Jama* **318**, 1550-1560 %@ 0098-7484 (2017).
68 Shankaran, S. *et al.* Effect of depth and duration of cooling on death or disability at age 18 months among neonates with hypoxic-ischemic encephalopathy: a randomized clinical trial. *Jama* **318**, 57-67 %@ 0098-7484 (2017).
69 Jia, W., Lei, X., Dong, W. & Li, Q. Benefits of starting hypothermia treatment within 6 h vs. 6–12 h in newborns with moderate neonatal hypoxic-ischemic encephalopathy. *BMC pediatrics* **18**, 50 (2018).
70 Belliveau, J. W. *et al.* Functional mapping of the human visual cortex by magnetic resonance imaging. *Science* **254**, 716-719 %@ 0036-8075 (1991).
71 Lecrux, C. & Hamel, E. The neurovascular unit in brain function and disease. *Acta physiologica* **203**, 47-59 %@ 1748-1708 (2011).
72 Thompson, J. K., Peterson, M. R. & Freeman, R. D. Single-neuron activity and tissue oxygenation in the cerebral cortex. *Science* **299**, 1070-1072 %@ 0036-8075 (2003).
73 Raichle, M. E. & Gusnard, D. A. Appraising the brain's energy budget. *Proceedings of the National Academy of Sciences* **99**, 10237-10239 %@ 10027-18424 (2002).
74 Mergenthaler, P., Lindauer, U., Dienel, G. A. & Meisel, A. Sugar for the brain: the role of glucose in physiological and pathological brain function. *Trends in neurosciences* **36**, 587-597 %@ 0166-2236 (2013).
75 McHedlishvili, G. I. *Arterial behavior and blood circulation in the brain*. (Plenum Pub Corp, 1986).
76 Hamel, E. Perivascular nerves and the regulation of cerebrovascular tone. *Journal of applied physiology* **100**, 1059-1064 %@ 8750-7587 (2006).
77 Hendrikx, D. *et al.* Measurement of Neurovascular Coupling in Neonates. *Front Physiol* **10**, 65, doi:10.3389/fphys.2019.00065 (2019).
78 Iadecola, C. Neurovascular regulation in the normal brain and in Alzheimer's disease. *Nature Reviews Neuroscience* **5**, 347-360 %@ 1471-0048 (2004).
79 Huneau, C., Benali, H. & Chabriat, H. Investigating human neurovascular coupling using functional neuroimaging: a critical review of dynamic models. *Frontiers in neuroscience* **9**, 467 %@ 1662-1453X (2015).
80 Phillips, A. A., Chan, F. H. N., Zheng, M. M. Z., Krassioukov, A. V. & Ainslie, P. N. Neurovascular coupling in humans: physiology, methodological advances and clinical implications. *Journal of Cerebral Blood Flow & Metabolism* **36**, 647-664 %@ 0271-0678X (2016).
81 Mosso, A. *Ueber den Kreislauf des Blutes im menschlichen Gehirn*. (Veit, 1881).
82 Kozberg, M. & Hillman, E. in *Progress in brain research* Vol. 225 213-242 %@ 0079-6123 (Elsevier, 2016).
83 Govindan, R. B., Massaro, A., Chang, T., Vezina, G. & du Plessis, A. A novel technique for quantitative bedside monitoring of neurovascular coupling. *Journal of neuroscience methods* **259**, 135-142 %@ 0165-0270 (2016).
84 Caicedo, A. *et al.* in *Oxygen Transport to Tissue XXXVIII* 143-149 (Springer, 2016).
85 Hendrikx, D. *et al.* in *Oxygen Transport to Tissue XLI* 11-17 (Springer, 2020).

86 Ahmed, R., Temko, A., Marnane, W. P., Boylan, G. & Lightbody, G. Exploring temporal information in neonatal seizures using a dynamic time warping based SVM kernel. *Computers in biology and medicine* **82**, 100-110 (2017).
87 Gupta, L. & Srinath, M. D. Invariant planar shape recognition using dynamic alignment. *Pattern Recognition* **21**, 235-239 (1988).
88 Hüning, B. *et al.* Relationship between brain function (aEEG) and brain structure (MRI) and their predictive value for neurodevelopmental outcome of preterm infants. *European journal of pediatrics* **177**, 1181-1189 %@ 0340-6199 (2018).
89 Hamelin, S., Delnard, N., Cneude, F., Debillon, T. & Vercueil, L. Influence of hypothermia on the prognostic value of early EEG in full-term neonates with hypoxic ischemic encephalopathy. *Neurophysiologie Clinique/Clinical Neurophysiology* **41**, 19-27 %@ 0987-7053 (2011).
90 Dereymaeker, A. *et al.* Automated EEG background analysis to identify neonates with hypoxic-ischemic encephalopathy treated with hypothermia at risk for adverse outcome: A pilot study. *Pediatrics & Neonatology* **60**, 50-58 %@ 1875-9572 (2019).
91 Burton, V. J. *et al.* A pilot cohort study of cerebral autoregulation and 2-year neurodevelopmental outcomes in neonates with hypoxic-ischemic encephalopathy who received therapeutic hypothermia. *BMC neurology* **15**, 1-13 %@ 1471-2377 (2015).